A unified Hapke-HSR + MARMIT-2 soil radiative transfer model for reflectance simulation under varying moisture conditions

Anxin Ding[1,2], Han Ma[3], Shunlin Liang[3*], Ziti Jiao[4,5], Alexander A.Kokhanovsky[6], Hanyu Shi[7], Rui Xie[8]

[1]Key Laboratory of Humid Subtropical Eco-Geographical Process (Ministry of Education), Fujian Normal University, Fuzhou 350000, China

[2]School of Geographical Sciences, School of Carbon Neutrality Future Technology, Fujian Normal University, Fuzhou 350000, China

[3]Jockey Club STEM Laboratory of Quantitative Remote Sensing, Department of Geography, University of Hong Kong, Hong Kong 999077, China

[4]State Key Laboratory of Remote Sensing and Digital Earth, Faculty of Geographical Science, Beijing Normal University, Beijing 100875, China

[5]Faculty of Geographical Science, Institute of Remote Sensing Science and Engineering, Beijing Normal University, Beijing 100875, China

[6]Philipps-Universität Marburg Department of Geography Laboratory for Climatology and Remote Sensing F|14, Deutschhausstr. 1235032 Marburg, Germany

[7]School of Geospatial Artificial Intelligence, East China Normal University, Shanghai 200241, China.

[8]International Institute for Earth System Sciences, and School of Geography and Ocean Science, Nanjing University, Nanjing 210023, China.

Correspondence to: Shunlin Liang (shunlin@hku.hk)

Abstract. Soil radiative transfer models (RTMs) provide a physical basis for interpreting surface reflectance and retrieving land-surface parameters. However, most existing soil RTMs represent either the spectral-directional scattering behavior of dry soils or the moisture-induced absorption effects of wet soils, and a physically consistent formulation capable of jointly describing both processes remains limited. In this study, we develop a unified soil RTM by refining the Hapke-based hyperspectral reflectance model (Hapke-HSR) using dry soil reflectance and dynamically coupling it with the improved multilayer RTM of soil reflectance (MARMIT-2). The proposed Hapke-HSR + MARMIT-2 model explicitly represents the interaction between particle scattering and moisture-dependent absorption and refraction processes, enabling joint spectral-directional simulation of soil reflectance under varying soil moisture conditions. The model is systematically evaluated using eight independent soil spectral databases spanning a wide range of textures and moisture levels. Results show that the Hapke-HSR + MARMIT-2 model consistently improves simulation accuracy and stability relative to the individual Hapke-HSR and MARMIT-2 models, with particularly pronounced gains at high soil moisture regimes (SMC ≥ 30%). Across all datasets, the proposed model achieves higher performance (R^2 = 0.993, RMSE = 0.007) than MARMIT-2 (R^2 = 0.983, RMSE = 0.012) and Hapke-HSR (R^2 = 0.909, RMSE = 0.028). The proposed framework provides a physically interpretable and extensible basis for soil reflectance modeling and offers a robust foundation for future developments in multi-angular hyperspectral remote sensing and land-surface parameter inversion.

Keywords: Soil radiative transfer model, soil reflectance, Hapke-HSR model, MARMIT-2 model, soil moisture content

1 Introduction

Soils are fundamental components of the Earth's surface system and play a critical role in agricultural productivity, ecosystem functioning, and hydrological processes (Fan et al., 2025; Rizzo et al., 2023; Shoshany et al., 2022). Soil reflectance is governed by a range of physical properties, including soil moisture content (SMC), particle size, and surface roughness, which jointly regulate the scattering and absorption of solar radiation (Gholami et al., 2018; Labarre et al., 2019;

Nolin and Liang, 2008; Sheng et al., 2024). Among these factors, SMC is one of the most influential and dynamic variables, exerting a dominant control on soil spectral behavior, particularly in the shortwave infrared region where water absorption features are pronounced (Bablet et al., 2019; Jiang and Fang, 2019; Xu et al., 2025). Because soil reflectance constitutes a fundamental component of optical remote sensing signals, a physically consistent soil radiative transfer model is essential for reliably linking observed reflectance to soil and vegetation parameters and for supporting the inversion of land-surface biophysical variables (Gao et al., 2024; Lei et al., 2025; Yang et al., 2025).

Soil radiative transfer models (RTMs) describe the absorption, scattering, and transmission of solar radiation within soil media and provide a physically based framework for linking surface reflectance to soil properties (Bach and Mauser, 1994; Jacquemoud, 1992; Liang and Townshend, 1996a, b; Sadeghi et al., 2007). Owing to their explicit physical formulation, RTMs have become a fundamental tool for the inversion of soil-related parameters from optical remote sensing observations. Moreover, soil reflectance constitutes a key background component of vegetation canopies and directly affects the accuracy of vegetation radiative transfer models and the retrieval of biophysical vegetation variables (Ni and Li, 2000; Ma et al., 2017a, b; Yang, 2022; Zeng et al., 2021). Despite substantial progress, important limitations remain in current soil RTMs. Many widely used models, including the multilayer radiative transfer model of soil reflectance (MARMIT) (Bablet et al., 2019) and the brightness-shape-moisture (BSM) model (Verhoef et al., 2018), rely on simplified assumptions of soil reflectance behavior and do not fully capture the combined spectral variability and moisture-dependent effects of natural soils (Jiang and Fang, 2019; Yang, 2022). Consequently, the development of physically consistent soil RTMs that can jointly represent spectral behavior and moisture-driven processes remains a critical requirement for reliable surface radiative transfer modeling and parameter inversion (Cheng et al., 2022; Jiang et al., 2023; Li et al., 2021; Verhoef et al., 2007). To address this requirement, appropriate model selection is essential for constructing a physically consistent framework. Among the soil models listed in Table 1, the Hapke-HSR and MARMIT-2 models were selected due to their complementary physical characteristics. The Hapke-HSR model explicitly represents directional scattering and provides a physically based description of dry soil reflectance, whereas the MARMIT-2 model focuses on moisture-related absorption processes but does not account for angular effects and depends on externally prescribed dry soil reflectance. Their combination therefore enables a physically consistent integration of directional and moisture-dependent processes, which is not achievable with semi-empirical models such as the BSM model.

Table 1. Summary of the strengths and limitations of existing soil radiative transfer models.

Models/References	Modelling dry soil	Absorption of water film	Irregular water film thickness	BRDF signatures
Ångström (Ångström, 1925)	×	√	×	×
Lekner & Dorf (1988)	×	√	×	×
Bach & Mauser (1994)	×	√	×	×
SPLITS (Kimmel & Baranoski, 2007)	√	√	√	√
Hapke (2012)	√	√	×	√
Sadeghi et al.(2017)	×	√	×	×
BSM (Verhoef et al., 2018)	√	√	√	×
MARMIT (Bablet et al., 2018)	×	√	√	×
Hapke-HSR (Ding et al., 2022)	√	√	×	√
MARMIT-2 (Dupiau et al., 2022)	×	√	√	×

The Hapke model has been widely applied in remote sensing for the retrieval of soil physical and biochemical properties (Hapke, 2012; Zhao et al., 2023). Building on this framework, we previously developed a hyperspectral Hapke model (i.e, the Hapke-HSR model) by establishing a wavelength-dependent representation of the single scattering albedo (SSA) (Ding et al., 2022), which enables improved simulation of dry soil spectral reflectance (SSR). Nevertheless, important limitations remain in the representation of moisture-dependent soil reflectance. First, the Hapke-HSR model is primarily

parameterized for dry soil conditions, and its extension to wet soils relies on simplified assumptions. Second, the influence of soil moisture is represented through an idealized surface water layer, which restricts the model's ability to accurately characterize reflectance variations across a broad range of soil moisture content (SMC) and leads to systematic biases in major water absorption regions. Recently, the MARMIT-2 model has demonstrated strong performance in simulating SSR under varying moisture conditions by incorporating reflectance properties from diverse soil types (Dupiau et al., 2022). However, the MARMIT-2 model does not explicitly represent angular effects and requires prior knowledge of dry soil reflectance, which is often difficult to obtain from field or satellite observations. These limitations indicate that neither Hapke-HSR nor MARMIT-2 model alone provides a fully consistent framework for modeling soil reflectance under varying moisture conditions, thereby motivating the development of a unified soil modeling framework.

To address these limitations, this study develops a unified soil radiative transfer framework by coupling the improved Hapke-HSR model with the MARMIT-2 model. The main contributions can be summarized as follows. First, the proposed framework integrates directional scattering and moisture-related absorption processes within a physically consistent formulation, which is not achieved by existing models. Second, the improved Hapke-HSR model dynamically provides dry soil reflectance, thereby removing the dependency of MARMIT-2 model on externally prescribed dry reflectance. Third, the coupled model enhances simulation robustness under high soil moisture conditions, particularly in strong water absorption regions. Overall, this study presents a unified and physically interpretable framework for simulating soil reflectance under varying moisture conditions, improving both consistency and applicability for remote sensing inversion.

2 Soil radiative transfer models

2.1 Hapke-HSR model

In the Hapke-HSR model, dry soil is treated as a semi-infinite horizontal surface containing irregularly and randomly distributed absorbing particles (Ding et al., 2022), and the formulas of this model are defined as follows:

$$R_d(\theta_s,\theta_v,\phi,\lambda)=\frac{\omega}{4}\frac{1}{\cos\theta_s+\cos\theta_v}\{[P(g,g')(1+B(g))]+H(\cos\theta_s)H(\cos\theta_v)-1\} \tag{1}$$

$$P(g,g')=1+b\cos g+\frac{c(3\cos^2 g-1)}{2}+b'\cos g'+\frac{c'(3\cos^2 g'-1)}{2} \tag{2}$$

$$\cos g=\cos\theta_s\cos\theta_v+\sin\theta_s\sin\theta_v\cos\phi \tag{3}$$

$$\cos g'=\cos\theta_s\cos\theta_v-\sin\theta_s\sin\theta_v\cos\phi \tag{4}$$

$$B(\mathrm{g})=\frac{B_0}{1+\frac{1}{h}\tan(\frac{g}{2})} \tag{5}$$

$$H(x)=\frac{1+2x}{1+2x\sqrt{1-\omega}} \tag{6}$$

where $R_d(\theta_s, \theta_v, \varphi, \lambda)$ represents dry soil reflectance, and ω denotes the average SSA. B(g)) is the hotspot function, with B_0 = 0.4 and h = 0.1 adopted as optimal values. The scattering phase function is represented by P(g, g'), for which the parameters are set as b' = 0.4, c = 0.4, and c' = 0. These parameter values are adopted from previous studies (e.g., Hapke, 2012; Ding et al., 2022) and represent commonly used or empirically optimized values for soil surfaces, providing stable and physically reasonable simulations across a wide range of conditions. The P(g, g') function is employed in this study because it provides an improved representation of soil anisotropic scattering characteristics. Here, θ_s, θ_v, and φ denote the solar zenith angle (SZA), view zenith angle (VZA), and relative azimuth angle (RAA), respectively.

The relationship between the soil SSA and wavelength was established via radiative transfer theory. The association formulas of the SSA and wavelength are as follows:

$$\omega = 1 - \frac{4\pi M \chi_{soil}}{\lambda} \tag{7}$$

where M represents the soil particle size and shape-dependent parameter and χ_{soil} is the soil refractive index, which is important for simulating soil optical properties.

In the Hapke-HSR model, the relationship between SSA (ω) and wavelength is further simplified as follows:

$$\omega_1 = 1 - \frac{1}{A_0\lambda + A_1} \tag{8}$$

$$\omega_2 = 1 - \frac{1}{A_2\lambda + A_3} + \Delta d \tag{9}$$

where Δd refers to the offset of two soil spectra and where A_0, A_1, A_2 and A_3 represent the soil spectral parameters.

Considering the influence of SMC, we assume that the equivalent water thickness represents the transition from dry soil to wet soil (Yang et al., 2011). The formulas are defined as follows:

$$R_w(\theta_s, \theta_v, \phi, \lambda) = R_d(\theta_s, \theta_v, \phi, \lambda) \times e^{-\alpha_{water} f} \tag{10}$$

$$\alpha_{water} = \frac{4\pi\chi_{water}}{\lambda} \tag{11}$$

where $R_w(\theta_s, \theta_v, \varphi, \lambda)$ represents wet soil reflectance, χ_{water} is the water refractive index for water, and f is the equivalent water thickness.

2.2 Improvement of the Hapke-HSR model

The primary challenge in addressing the statistical relationship between the SSA and wavelength of the Hapke-HSR model is to provide a stable parameter χ_{soil}. In this study, we assume that the shape of the dry SSR is consistent with the variation in the SSA with wavelength (Ding et al., 2022). A method is proposed to calculate the parameter χ_{soil} via the dry SSR and improve the Hapke-HSR model. The SSA typically has a significant influence on the SSR, with multiple scattering events often disregarded in the theoretical derivation (Yang, 2022). The relationships between dry SSR and SSA are as follows:

$$R_d(\theta_s, \theta_v, \phi, \lambda) = C_1 \times \omega \tag{12}$$

$$C_1 = \frac{1}{4(\cos\theta_s + \cos\theta_v)} \{[P(g, g')(1 + B(g))] - 1\} \tag{13}$$

$$\omega = 1 - \frac{C_2 \times \chi_{soil}}{\lambda} \tag{14}$$

$$C_2 = 4\pi M \tag{15}$$

$$\chi_{soil} = \frac{\lambda}{C_2} \times (1 - \frac{R_d(\theta_s, \theta_v, \phi, \lambda)}{C_1}) \tag{16}$$

where C_1 and C_2 are the shape adjustment parameters of the dry SSR. We use C_1 = 1 and C_2 = 1 as the initial values to simplify the calculation, and we then further calculate the shape adjustment parameters.

To incorporate the impact of multiple scattering within the soil, we first calculate the χ_{soil} parameter via Eq. (16). This parameter is then utilized in the improved Hapke-HSR model to determine the dry SSR. We adjust the dry SSR estimated with the improved Hapke-HSR model via the measured SSR and then calculate the adjusted dry SSR. The relationship

between the dry SSR simulated via the improved Hapke-HSR model and the measured dry SSR can be expressed via the following formula:

$$R_d^{'}(\theta_s,\theta_v,\phi,\lambda) = C_3 \times R_d(\theta_s,\theta_v,\phi,\lambda) + C_4 \quad (17)$$

where C_3 and C_4 are spectral shape adjustment parameters for dry soil reflectance, obtained through linear regression between simulated and measured reflectance, and used as empirical correction terms to compensate for discrepancies arising from the simplified treatment of multiple scattering in the Hapke-HSR model. Here, $R_d(\theta_s, \theta_v, \varphi, \lambda)$ denotes the reflectance simulated by the improved Hapke-HSR model, and $R'_d(\theta_s, \theta_v, \varphi, \lambda)$ represents the measured dry soil reflectance.

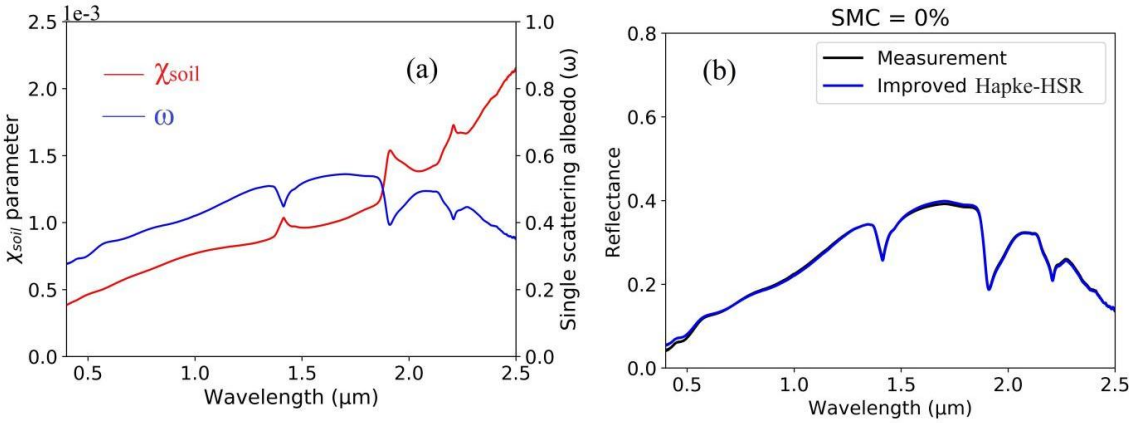

Figure 1: The variation in the soil refractive index (parameter χ_{soil}) and SSA of dry soil with wavelength (a). The measured dry soil reflectance (i.e., dup20_009) and soil reflectance calculated with the improved Hapke-HSR model (b).

Figure 1(a) shows the variation in the parameter χ_{soil} and soil SSA calculated with the dry SSR (i.e., dup20_009) considering the wavelength. The parameter χ_{soil} increases with wavelength, the slope clearly increases at wavelengths of 2.0–2.5 μm, and there are obvious peak values in the absorption band of water (centred at 1.47, 1.90 and 2.21 μm). The soil SSA is highly similar to the dry SSR. With increasing wavelength, the SSA increases significantly in the spectral range of 0.4–1.36 μm. In the spectral range of 1.36–2.5 μm, obvious valleys occur in the absorption band of water, which is similar to that of dry SSR. In general, the SSA and dry SSR curves display very high similarity in terms of shape, but the SSA curve is flatter. Figure 1(b) shows the measured dry SSR and the SSR estimated with the improved Hapke-HSR model. Clearly, the SSR modelled by the improved Hapke-HSR model matches well with the measured dry SSR and can characterize the dry SSR characteristics well. The accuracy of this improved model in fitting these typical data is shown in Table 4 (R^2 = 1.00, RMSE = 0.001). These analyses suggest that calculating the parameter χ_{soil} via dry SSR data is feasible and can solve the problems associated with the statistical relationship between the SSA and wavelength of the Hapke-HSR model.

2.3 Coupling strategy between the improved Hapke-HSR and MARMIT-2 models

(1) Physical coupling mechanism between the improved Hapke-HSR model and MARMIT-2 model

The improved Hapke-HSR model provides an effective description of multi-angular dry soil spectral reflectance, whereas the MARMIT-2 model explicitly accounts for the influence of SMC on soil reflectance but assumes that dry reflectance is known and does not incorporate directional information. By coupling these two models, their complementary strengths can be integrated to achieve a more physically consistent representation of both the spectral and moisture-dependent behavior of soils. In the proposed framework, dry soil reflectance under different viewing geometries is first simulated using the improved Hapke-HSR model and subsequently used as input to the MARMIT-2 model. As a result, the MARMIT-2 model no longer requires externally prescribed dry reflectance. Moreover, because the simulations of the Hapke-HSR model retain angular information, the coupled Hapke-HSR + MARMIT-2 model is able to account for the influence of observation

geometry on soil reflectance. Through this coupling strategy, the reflectance properties of both dry and wet soils can be simulated under varying angular and moisture conditions within a unified framework (Ding, 2025).

(2) Radiative transfer formulation of the coupled Hapke-HSR + MARMIT-2 model

In the MARMIT-2 model, wet soil is described as dry soil overlaid with a thin layer of water (Dupiau et al., 2022). Therefore, the wet SSR is described as follows:

$$R_{mod}(\theta_s,\theta_v,\phi,\lambda)=\varepsilon R_w(\theta_s,\theta_v,\phi,\lambda)+(1-\varepsilon)R_d(\theta_s,\theta_v,\phi,\lambda) \quad (18)$$

where $R_m(\theta_s, \theta_v, \varphi, \lambda)$ is the wet SSR, $R_d(\theta_s, \theta_v, \varphi, \lambda)$ is the dry SSR calculated via the improved Hapke-HSR model, $R_w(\theta_s, \theta_v, \varphi, \lambda)$ refers to the fully wet SSR, ε is the wet soil fraction, and $R_w(\theta_s, \theta_v, \varphi, \lambda)$ is described as:

$$R_w(\theta_s,\theta_v,\phi,\lambda)=\frac{t_{12}t_{21}R_d(\theta_s,\theta_v,\phi,\lambda)T_w^2}{1-r_{21}R_d(\theta_s,\theta_v,\phi,\lambda)T_w^2} \quad (19)$$

where t_{12} and t_{21} are the interface transmittance of light passing into and out of the water layer, respectively.

To address the presence of multiple scattering events within the water layer, transmittance (T_w) is considered.

$$T_w=(1-\alpha_{water}L)e^{-\alpha_{water}L}+\alpha_{water}L\int_{\alpha_{water}L}^{\infty}\frac{e^{-x}}{x}dx \quad (20)$$

where L refers to the water layer thickness.

$$n_{mix}=\delta n_{soil}+(1-\delta)n_{water} \quad (21)$$

where n_{mix} represents the result of the linear weighting of the complex refractive index of water and soil, n_{soil} and n_{water} represents the complex refractive index of water and soil particles respectively, and δ represents the volume fraction of soil particles.

(3) Computational procedure and evaluation scheme

Figure 2 illustrates the workflow of the improved Hapke-HSR model and its coupling with the MARMIT-2 model. First, the soil parameter χ_{soil} is estimated from measured dry SSR by assuming similarity between the spectral shapes of the single-scattering albedo and dry SSR. The derived χ_{soil} is then incorporated into the Hapke-HSR model, which alleviates the limitations associated with piecewise fitting of the single scattering albedo and improves the numerical stability of the formulation. The refined Hapke-HSR model is subsequently used to simulate dry SSR under different viewing geometries, and these simulations are provided as input to the MARMIT-2 model, thereby enabling the dynamic coupling of the two formulations. For parameter estimation, the coupled model allows flexible inversion strategies. In this study, the parameters can be estimated either simultaneously by jointly optimizing all model parameters, or sequentially by first determining the dry-soil scattering parameters (e.g., b and M) using the Hapke-HSR model, followed by the estimation of moisture-related parameters (e.g., ε, L and δ) using the MARMIT-2 model. Finally, the performance of the coupled Hapke-HSR + MARMIT-2 model is evaluated using eight independent soil spectral databases spanning a range of soil moisture conditions. Model performance is assessed using multiple statistical metrics, including the coefficient of determination (R^2), root mean square error (RMSE), normalized RMSE (NRMSE), mean relative error (MRE), and bias.

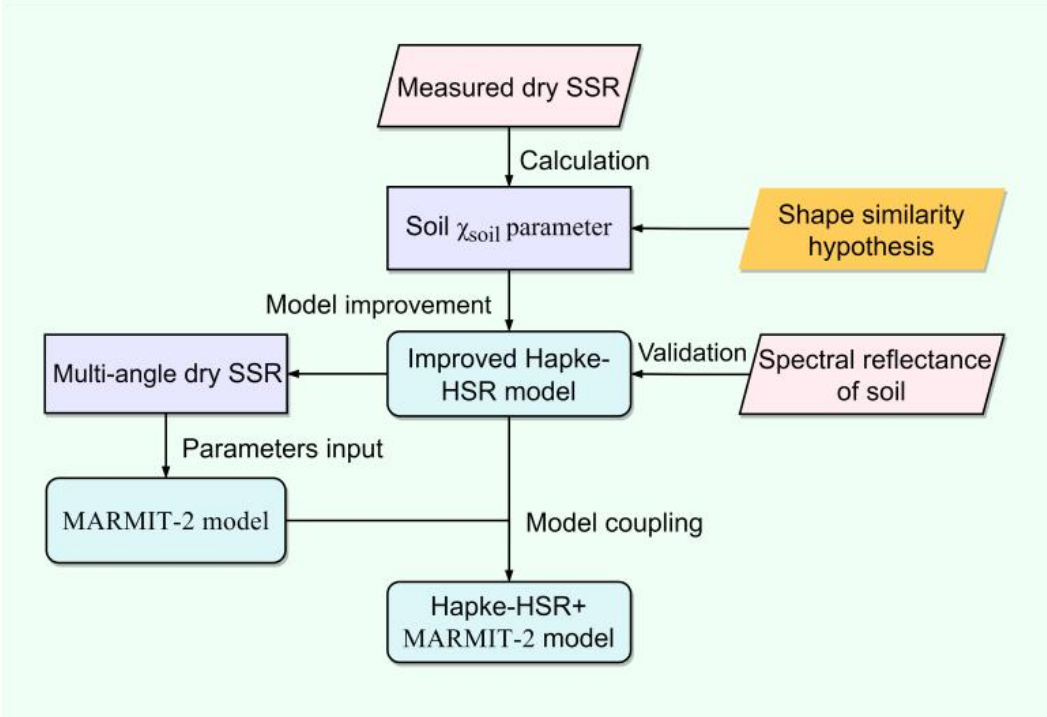

Figure 2: The workflow of the improved Hapke-HSR model and the coupled MARMIT-2 model.

3 Databases and methods

3.1 Databases of soil spectral reflectance

In this section, eight different databases provided by Dupiau et al. (2022) are used to verify the Hapke-HSR + MARMIT-2 model (Table 2). These eight datasets were acquired primarily via the Analytical Spectra Devices (ASD) FieldSpec spectroradiometer. The soil types in the datasets are diverse, consisting primarily of clay, silt, and sand as the main components. The Bab16, Dup20, and Liu02 databases provide the soil components of each sample, such as organic matter, iron, nitrogen and organic carbon. These eight databases provide dry and wet SSR data for 219 soil samples, spanning 1984 spectra in the 0.4-2.5 μm range. The data quality of these databases is high, but there are some uncertainties in the 2.4-2.5 μm range. Therefore, these databases offer crucial data for validating the ability of the Hapke-HSR + MARMIT-2 model to describe SSR features.

Table 2. The main information on the eight soil databases.

Databases	Locations	Number of soil spectrum	Spectral range (μm)	Spectral resolution (μm)	SMCg (%)
Bab16	ONERA, Toulouse (France)	106	0.4-2.4	0.001	0-79.2
Dup20	ONERA, Toulouse (France)	72	0.4-2.5	0.001	0-68.91
Hum15	ONERA, Toulouse (France)	455	0.4-2.298	0.001	0-67
Les08	ONERA, Toulouse (France)	190	0.4-2.4	0.001	0-87
Liu02	INRAE, Avignon (France)	367	0.4-2.4	0.001	0-81.1
Lob02	Standford University, Standford (CA, USA)	41	0.4-2.49	0.001	0-109.4
Mar12	CEA, Bruyères le Chatel (France)	258	0.4-2.4	0.001	0-52.9
Phil14	Cornell University, Ithaca (NY, USA)	405	0.4-2.5	0.001	0-50.71

Note: SMCg is the soil moisture content (SMC) as a weight percent.

4 Results and analysis

4.1 Parameters analysis of the Hapke-HSR + MARMIT-2 model

In this section, we first analyse the effects of the main input parameters of the Hapke-HSR + MARMIT-2 (HM) model on the soil reflectance properties. Table 3 shows the main input variables of the HM model. The Hapke-HSR model has many input variables, and the variables of this model were optimized in previous studies (Ding et al., 2022; Dupiau et al., 2022; Hapke, 2012; Verhoef et al., 2018); five main variables were used to describe the soil spectral and angular features. The MARMIT-2 model includes three main parameters that describe the influence of the SMC on SSR. We analyse the effects of different parameters in the HM model on the simulated SSR.

Table 3. The main input variables of the Hapke-HSR + MARMIT-2 (HM) model.

Databases	Parameters	Range of values	Units
Hapke-HSR	Solar zenith angle (SZA)	0-90	degrees (°)
	View zenith angle (VZA)	0-90	degrees (°)
	Relative azimuth angle (RAA)	0-180	degrees (°)
	The coefficient of the scattering phase function (b)	0-6	--
	Soil particle size and shape-dependent parameter (M)	0-1	mm
MARMIT-2	Volume fraction of soil particles (δ)	0-0.25	--
	Thickness of water layer (L)	0-0.15	cm
	Surface coverage fraction of water (ε)	0-1	--

Figure 3 illustrates the impact of the main variables of the Hapke-HSR + MARMIT-2 (HM) model on the SSR. For the influence of angle variation, the SSR calculated via the HM model increases with increasing SZA parameters. The increase in SSR is obvious in the range of 0.4–1.36 μm; however, the rate of increase in SSR subsequently decreases. The impact of VZA parameters on SSR is consistent with the influence of the SZA parameters since the Hapke-HSR model is reciprocal. Furthermore, the influence of the RAA parameters on SSR is basically the same as that of the SZA parameters with increasing RAA parameters; however, the changes in soil reflectance are slightly different. With increasing parameter b, the SSR simulated by the HM model decreases, with a more pronounced reduction in the range of 0.4–1.36 μm than in 1.36–2.5 μm. Both parameters b and c influence the BRDF shape through the phase function. However, b primarily controls the overall anisotropy of scattering, whereas c governs the forward–backward asymmetry. Under the observational configurations considered in this study, b shows a stronger and more stable influence on reflectance, while the sensitivity of c is relatively weaker. Therefore, the discussion focuses on parameter b (Ding et al., 2022, 2026). The SSR simulated with the HM model also decreases with increasing M; this finding corroborates the experimental observations regarding spectral variations due to soil particle size reported by Sun et al.(2023). However, the variation in the parameter M of the SSR is basically the same at different wavelengths. A possible reason is that the influence of the parameter M in the range of 0.4-2.5 μm on the SSR is consistent, which may be related to the structure of Eq. (7). For the variables related to the SMC, with increasing parameter δ, the SSR decreases, whereas in the strong absorption band of water, this effect is smaller. A possible reason for this result is that the absorption of water weakens the impact of the parameter δ on the SSR. As the parameter L increases, the SSR decreases in the range of 1.0–2.5 μm, whereas the variation in the parameter L has no effect on the soil reflectance in the range of 0.4–1.0 μm. With increasing parameter ε, the SSR decreases. In the strong absorption band of water, the simulated SSR quickly decreases. In summary, the main parameters of the Hapke-HSR model are related to the influence of dry SSR and angular variation characteristics, and the variables of the MARMIT-2 model mainly account for the influence of SMC on the SSR. Therefore, the HM model can characterize the spectral and angular reflectance attributes of dry and wet soils by coupling the Hapke-HSR and MARMIT-2 models.

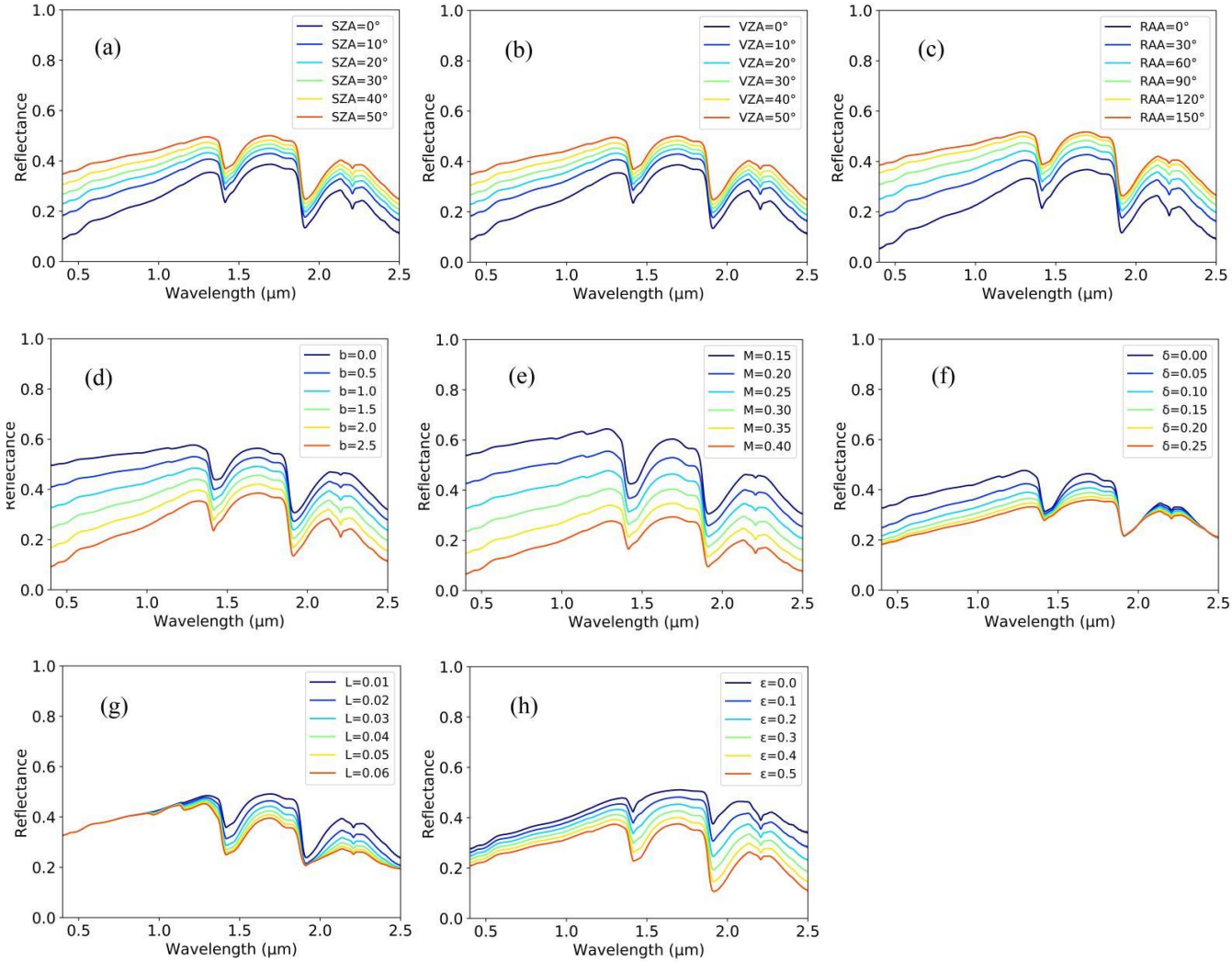

Figure 3: Influence of the SZA (a), VZA (b), RAA (c), *b* (d), *M* (e), *δ* (f), and *ε* (h) in the Hapke-HSR + MARMIT-2 (HM) model on soil reflectance.

4.2 Validating the Hapke-HSR + MARMIT-2 model to describe soil reflectance properties

In previous studies, we assessed the Hapke-HSR model to describe soil BRDF features (Ding et al., 2022). Therefore, we focus mainly on evaluating the soil spectral characteristics in this paper. In addition, these eight soil databases do not provide angle-related information. Therefore, we use SZA = 45°, VZA = 0° and RAA = 0° as fixed values because SSR is usually measured in the nadir direction. Figure 4 shows that the Hapke-HSR, MARMIT-2 and Hapke-HSR + MARMIT-2 (HM) models effectively fit the influence of the typical fitted SSR (dup20_009-001) at SMCs = 0%, 14.45%, 27.34%, 31.6%, 36.2%, 40.34%, 45.07%, 49.25%, and 57.06%, respectively. The SSR decreases significantly with increasing SMC, and the main absorption bands (centred at 1.47 and 1.90 μm) of water become wider. The outcomes simulated using the Hapke-HSR, MARMIT-2 and HM models can be used to determine the change in SSR with increasing SMC and are highly in line with the measured SSR values. On the basis of a comparison of the results, the HM model fits the measured SSR better than the Hapke-HSR and MARMIT-2 models do, especially at SMC ≥ 30%. Compared with the MARMIT-2 model, the HM model yields slightly better results. The main reason is that the MARMIT-2 model yields very high accuracy in characterizing SSR characteristics. The ability of the Hapke-HSR model to accurately fit the measured SSR decreases with increasing SMC. The correlation analysis results indicate that the fitting ability of these two models meets the relevant requirements. However, at SMC ≥ 30%, the fitting capability of the MARMIT-2 model is relatively low due to slight underestimations in the range of 0.4-1.36 μm, and there is an overestimation in the strong water absorption band; moreover, the Hapke-HSR model has

difficulty capturing the SSR characteristics in the absorption band of water, which leads to significant underestimation of the fitted SSR at a wavelength of approximately 1.90 μm. However, the HM model effectively considers the influence of these factors, resulting in high accuracy for characterizing SSR attributes. To show the differences between the SSR values simulated with these three models and the measured spectral reflectance values, we calculate the bias between them, as shown in Appendix Figure A1. In addition, the Hapke-HSR and HM models are applied to simulate the dry SSR, and the SSR simulated via the HM model is more consistent with the measured results than the SSR obtained with the Hapke-HSR model is.

Table 4 shows that the Hapke-HSR, MARMIT-2 and HM models fit the parameters and statistical results of the SSR. With increasing SMC, the parameters L and ε in the MARMIT-2 model increase significantly, whereas the parameter δ shows little variation. The parameter f increases significantly. Moreover, the SSR fitting accuracy of the Hapke-HSR and MARMIT-2 models decreases with increasing SMC, especially at SMC ≥ 30%. This finding may be because the MARMIT-2 model ignores the variations in soil scattering characteristics, particle size and shape with increasing SMC. In the Hapke-HSR model, a dry soil surface is overlaid with a water layer to reflect the influence of the SMC on the SSR. This simple assumption limits the ability of the Hapke-HSR model to fit the variable characteristics of the SMC. The overall R^2 values for the Hapke-HSR model in SSR fitting vary from 0.952 to 0.971, with RMSE values varying from 0.016 to 0.019, and the MARMIT-2 model achieves R^2 values between 0.957 and 0.995 in SSR fitting, with RMSE values ranging from 0.007 to 0.021 and negligible bias. These results indicate that these two models can effectively characterize the variation in SSR with SMC and yield high fitting accuracy. However, the HM model is accurate (RMSE = 0.008), presenting a high R^2 (R^2 = 0.991) and a small bias in relation to the measured SSR. This is because the HM model considers the variations in the soil scattering characteristics, particle size and particle shape with increasing SMC. Therefore, the HM model can effectively characterize the attributes of SSR and exhibits greater accuracy than the Hapke-HSR and MARMIT-2 models do, especially at SMC ≥ 30%.

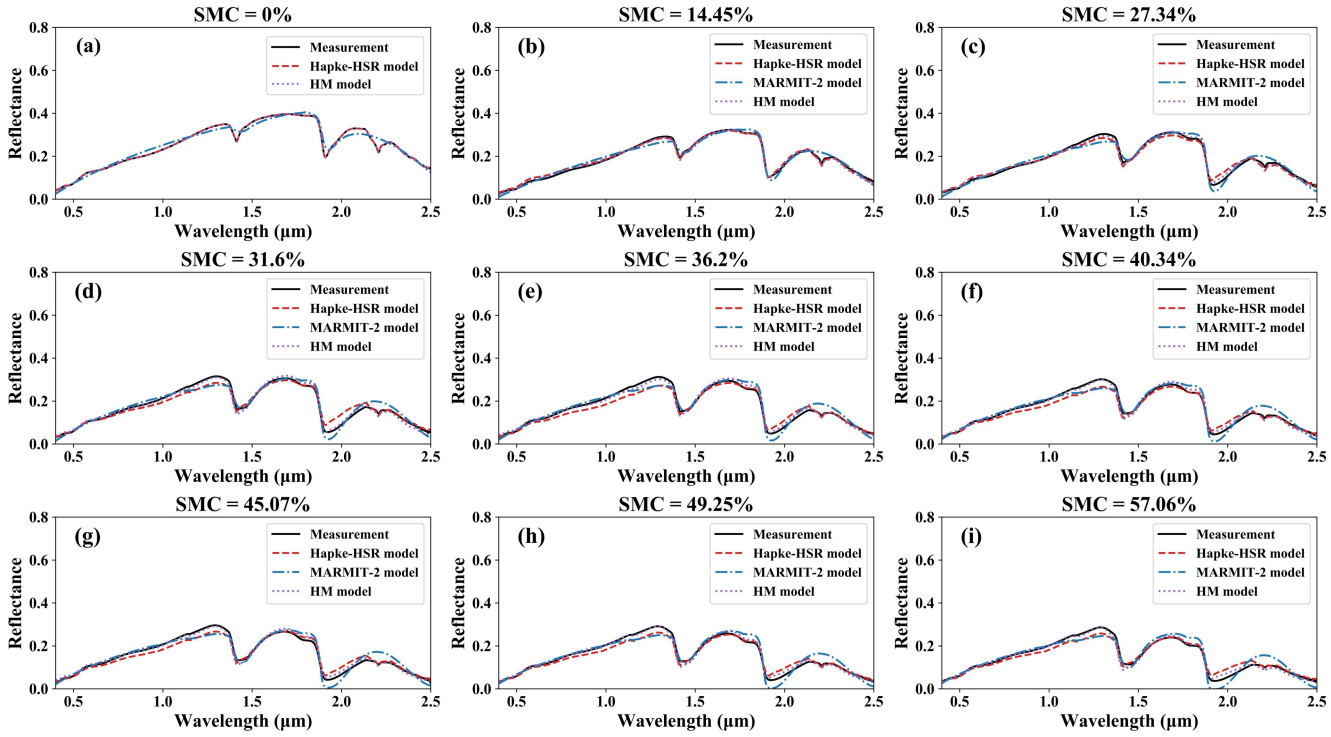

Figure 4: The Hapke-HSR (red), MARMIT-2 (blue) and Hapke-HSR + MARMIT-2 (HM) (lime) models fit the measured soil reflectance (black) at SMC = 0% (a), 14.45% (b), 27.34% (c), 31.6% (d), 36.2% (e), 40.34% (f), 45.07% (g), 49.25% (h), and 57.06% (i), respectively.

Table 4. The Hapke-HSR, MARMIT-2 and Hapke-HSR + MARMIT-2 (HM) models fit the soil reflectance variables and statistical outcomes.

Models	SMC (%)	b	f/M	A_0/δ	A_1/L	A_2/ε	A_3	R^2	RMSE	bias
Hapke-HSR	0.0	4.4	0.4	0.782	0.723	-1.141	4.178	0.972	0.016	0.001
	14.45	4.8	1.0	0.545	0.796	-0.708	3.054	0.976	0.013	0.001
	27.34	3.0	1.6	0.861	0.677	-1.151	4.336	0.968	0.016	0.000
	31.6	1.4	2.0	1.586	0.405	-1.908	6.738	0.962	0.019	0.001
	36.2	1.6	2.2	1.431	0.479	-1.795	6.326	0.954	0.020	0.002
	40.34	1.0	2.4	1.699	0.392	-1.924	6.948	0.948	0.020	0.002
	45.07	0.0	2.8	2.772	-0.009	-2.420	9.426	0.945	0.021	0.001
	49.25	0.8	2.8	1.747	0.384	-1.757	6.801	0.938	0.022	0.001
	57.06	0.2	3.4	2.316	0.188	-1.390	7.026	0.936	0.023	0.001
	All	--	--	--	--	--	--	0.952	0.019	0.001
MARMIT-2	0	--	--	--	--	--	--	--	--	--
	14.45	--	--	0.030	0.01	0.3	--	0.995	0.007	0.001
	27.34	--	--	0.000	0.03	0.3	--	0.984	0.013	-0.002
	31.6	--	--	0.000	0.03	0.3	--	0.957	0.019	-0.002
	36.2	--	--	0.000	0.02	0.4	--	0.955	0.021	-0.008
	40.34	--	--	0.000	0.03	0.4	--	0.970	0.018	-0.008
	45.07	--	--	0.000	0.03	0.4	--	0.956	0.018	-0.003
	49.25	--	--	0.000	0.04	0.4	--	0.969	0.017	-0.005
	57.06	--	--	0.000	0.05	0.4	--	0.957	0.018	-0.002
	All	--	--	--	--	--	--	0.971	0.016	-0.003
Hapke-HSR + MARMIT-2	0	2.0	0.30	0.000	0.00	0.0	--	1.000	0.001	0.000
	14.45	2.2	0.29	0.018	0.01	0.3	--	0.994	0.006	-0.001
	27.34	3.1	0.24	0.011	0.02	0.4	--	0.991	0.008	0.000
	31.6	4.0	0.21	0.006	0.02	0.5	--	0.989	0.009	-0.001
	36.2	3.3	0.23	0.000	0.02	0.5	--	0.986	0.010	0.000
	40.34	4.0	0.21	0.006	0.03	0.5	--	0.987	0.009	0.000
	45.07	3.3	0.23	0.001	0.03	0.5	--	0.987	0.009	0.002
	49.25	4.0	0.21	0.005	0.04	0.5	--	0.986	0.009	0.001
	57.06	3.7	0.22	0.000	0.05	0.5	--	0.984	0.009	-0.001
	All	--	--	--	--	--	--	0.991	0.008	0.000

Figure 5 shows that the Hapke-HSR, MARMIT-2 and HM models fit the typical measured SSR (bab16_014-008) at SMC = 0%, 5%, 10.7%, 16%, 21.1%, 30.8%, and 45.5%, respectively. This set of typical data is suspected to have a specular reflection effect when SMC = 30.8% and 45.5%. Therefore, we further validate the capacity of the HM model for describing the relevant SSR attributes. The outcomes of the Hapke-HSR, MARMIT-2 and HM models match the typical measured SSR when the SMC < 30%. The Hapke-HSR and MARMIT-2 models cannot effectively consider the specular reflectance characteristics at high SMCs (SMC ≥ 30%), and the results of the HM model display greater consistency with the measured

SSR values. When the SMC is high and there is a specular reflectance effect, the fitting capability of the Hapke-HSR model is significantly underestimated in the range of 0.5-1.2 μm and two strong water absorption bands; moreover, there is a slight overestimation in the range of 1.5-1.9 μm. The outcomes of the MARMIT-2 model are marginally underestimated across the 0.4–1.36 μm interval, and there is a slight overestimation across the spectral interval of 1.36–2.5 μm, particularly in the strong water absorption region. The HM model can match the measured SSR well, especially at SMC = 30.8% and 45.5%, possibly because this model accounts for the specular scattering characteristics of high SMCs (SMC ≥ 30%) on the basis of the coefficient (b) and soil particle shape-dependent parameter (*M*). To better show the differences between the SSR values simulated with these three models and the measured SSR values, we calculate the bias between them, as shown in Appendix Figure A2. The results indicate that the HM model can describe SSR features effectively at SMC ≥ 30%, and the simulated values exhibit very high consistency with the measured SSR values.

Table 5 shows that the Hapke-HSR, MARMIT-2 and HM models fit to the SSR parameters and statistical results. The overall precision of the Hapke-HSR and MARMIT-2 models in terms of fitting measured SSR was high (R^2 = 0.943-0.946, RMSE = 0.006-0.022), especially at SMC < 30%; however, these two models were not suitable at SMC ≥ 30%, which needs to be improved by accounting for specular reflectance. The HM model shows greater accuracy in fitting the variation in the SMC than the Hapke-HSR and MARMIT-2 models; the overall R^2 is 0.995, the RMSE is 0.009, and the bias is negligible. When SMC = 30.8% and 45.5%, the measured SSR are suspected to have a specular reflection effect, and the HM model maintains a higher fitting precision (R^2 = 0.990-0.993, RMSE = 0.009) than the Hapke-HSR and MARMIT-2 models (R^2 = 0.846-0.973, RMSE = 0.019-0.053). These results indicate that these two models can be combined by coupling the Hapke-HSR and MARMIT-2 models (i.e., HM model), which can effectively determine the variation in SSR with increasing SMC, particularly in the presence of specular reflectance.

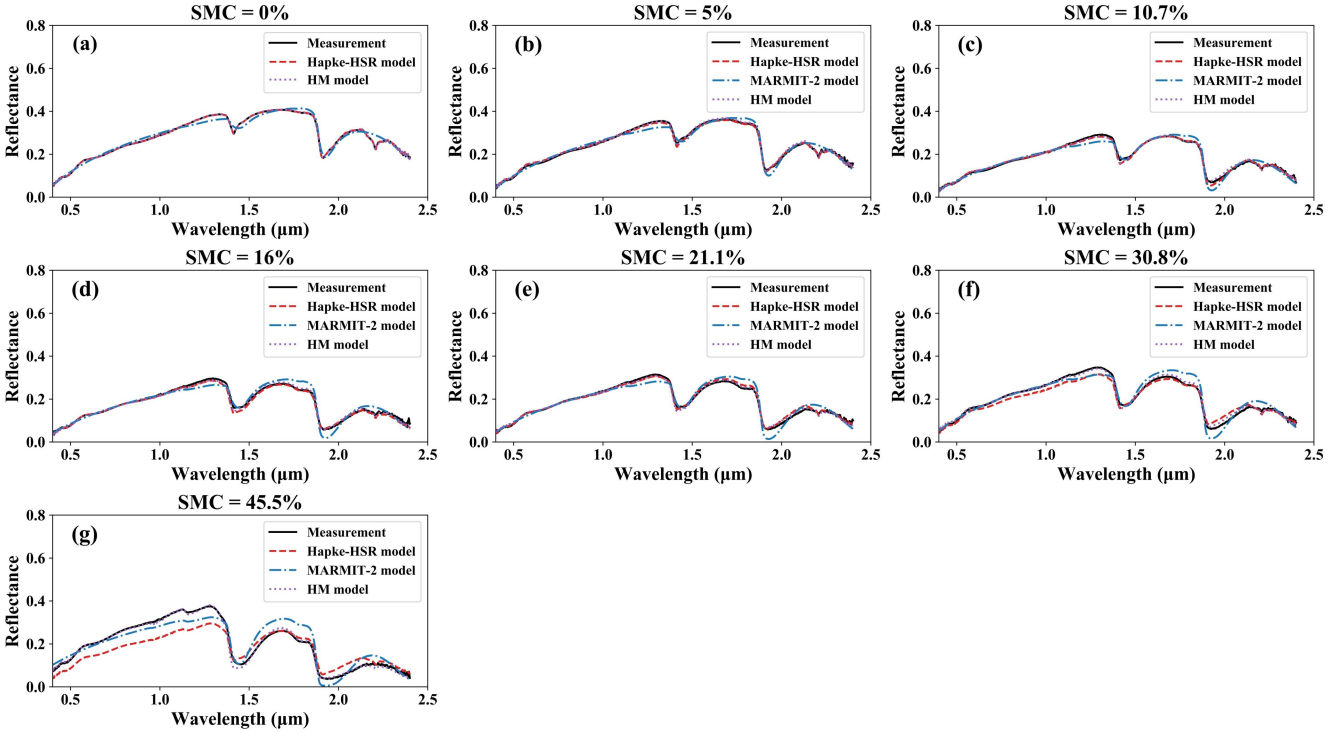

Figure 5: The Hapke-HSR (red), MARMIT-2 (blue) and Hapke-HSR + MARMIT-2 (HM) (lime) models fit the measured soil reflectance (black) at SMC = 0% (a), 5% (b), 10.7% (c), 16% (d), 21.1% (e), 30.8% (f), and 45.5% (g), respectively.

Table 5. The Hapke-HSR, MARMIT-2 and Hapke-HSR + MARMIT-2 (HM) models fit to the soil reflectance parameters and statistical results.

Models	SMC (%)	b	f/M	A_0/δ	A_1/L	A_2/ε	A_3	R^2	RMSE	bias
Hapke-HSR	0.0	1.4	0.6	2.447	0.180	-4.150	12.010	0.974	0.014	0.000
	5.0	1.4	1.0	2.016	0.322	-3.477	10.222	0.971	0.014	-0.001
	10.7	0.0	1.6	2.685	0.091	-5.119	14.339	0.960	0.015	-0.002
	16.0	0.2	2.0	2.506	0.189	-4.601	13.129	0.944	0.018	0.001
	21.1	0.0	2.2	3.144	-0.023	-5.618	15.939	0.941	0.020	0.000
	30.8	0.2	2.4	3.544	-0.173	-6.051	17.081	0.936	0.023	0.003
	45.5	1.0	4.0	2.377	0.439	-4.292	12.350	0.884	0.037	0.004
	All	--	--	--	--	--	--	0.943	0.022	0.001
MARMIT-2	0.0	--	--	--	--	--	--	--	--	--
	5.0	--	--	0.000	0.01	0.2	--	0.996	0.006	-0.001
	10.7	--	--	0.020	0.01	0.5	--	0.993	0.006	-0.001
	16.0	--	--	0.010	0.03	0.4	--	0.991	0.009	-0.005
	21.1	--	--	0.000	0.02	0.4	--	0.988	0.009	0.002
	30.8	--	--	0.000	0.04	0.3	--	0.973	0.019	-0.009
	45.5	--	--	0.000	0.04	0.4	--	0.846	0.053	-0.024
	All	--	--	--	--	--	--	0.946	0.022	-0.005
Hapke-HSR + MARMIT-2	0.0	2.0	0.30	0.000	0.00	0.0	--	1.000	0.001	0.000
	5.0	2.3	0.28	0.020	0.01	0.2	--	0.997	0.005	0.002
	10.7	1.3	0.38	0.001	0.02	0.3	--	0.994	0.006	0.000
	16.0	1.7	0.33	0.000	0.02	0.4	--	0.991	0.007	-0.001
	21.1	2.4	0.27	0.009	0.03	0.4	--	0.992	0.007	0.000
	30.8	3.0	0.24	0.002	0.03	0.4	--	0.990	0.009	0.002
	45.5	5.8	0.17	0.002	0.05	0.6	--	0.993	0.009	-0.002
	All	--	--	--	--	--	--	0.995	0.007	0.000

Figure 6 presents a comparison of the SSR results obtained from the Hapke-HSR, MARMIT-2 and HM models and the measured SSR values from eight databases. These three models are generally highly accurate in terms of capturing SSR features. However, the HM and MARMIT-2 models (R^2 = ~0.993) fit the measured SSR data with slightly greater correlation accuracy than did the Hapke-HSR model (R^2 = 0.957), and the RMSE values of the HM (RMSE = 0.010) and MARMIT-2 (RMSE = 0.012) models were significantly lower than the RMSE of the Hapke-HSR (RMSE = 0.027) model. Additionally, the MRE values of the HM and MARMIT-2 models are approximately 5.74% and 6.43% lower than that of the Hapke-HSR model, respectively. These findings indicate that the HM model yields the highest level of accuracy in fitting the measured SSR, followed by the MARMIT-2 model, whereas the Hapke-HSR model has the worst fitting effect on the basis of the measured SSR. The main reason is that the Hapke-HSR model includes a simple assumption regarding the effect of the SMC on SSR. In addition, the SSR simulated by the Hapke-HSR and MARMIT-2 models is considerably uncertain at high SMCs (e.g., Figure 5(f)-(g)), whereas the HM model results display greater consistency with the fitted SSR value. In general, the HM and MARMIT-2 models excellently characterize the SSR attributes of soil and yield greater accuracy than

the Hapke-HSR model for the eight soil databases does, and the SSR estimates produced by the HM model are marginally more accurate than those of the MARMIT-2 model are.

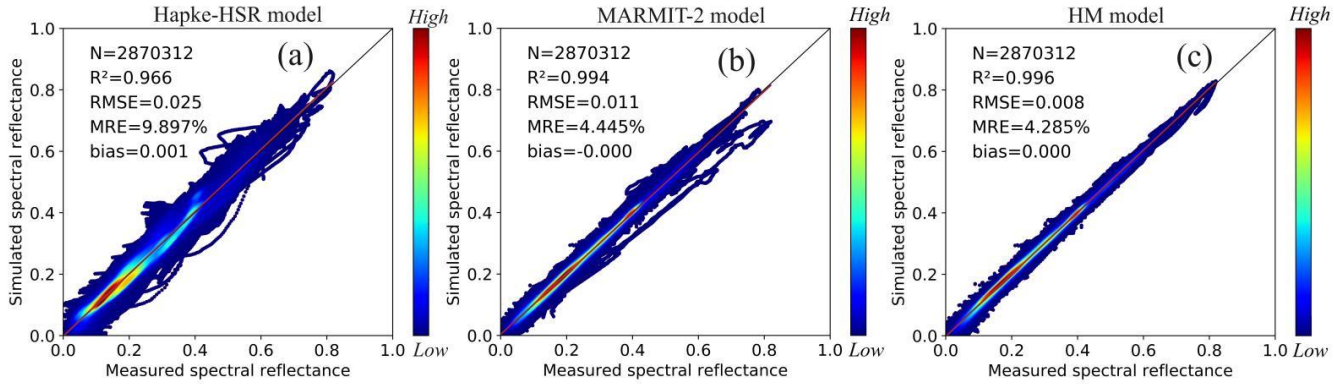

Figure 6: Comparison results of the all soil reflectance simulated by the Hapke-HSR (a), MARMIT-2 (b) and Hapke-HSR + MARMIT-2 (HM) (c) models with all measured soil reflectance.

4.3 Validating the Hapke-HSR + MARMIT-2 model for high SMC

The MARMIT-2 and HM models achieve excellent fitting accuracy at SMC levels ranging from 0-30%, whereas the Hapke-HSR and MARMIT-2 models exhibit moderate fitting capability at SMC ≥ 30% (e.g., Figures 3 and 4). Therefore, focus is placed on comparing the fitting results of the above three models under the condition of an SMC ≥ 30%. Figure 7 shows the comprehensive results obtained with the Hapke-HSR, MARMIT-2 and HM models at SMC ≥ 30%, and these three models exhibit strong agreement with the measured SSR (R^2 > 0.90), with RMSE values ranging from 0.0070.028. However, the accuracy of the HM model (R^2 = 0.993, RMSE = 0.007) for fitting SSR data is slightly better than that of the MARMIT-2 model (R^2 = 0.983, RMSE = 0.012) and significantly greater than that of the Hapke-HSR model (R^2 = 0.909, RMSE = 0.028). Compared with those of the MARMIT-2 and Hapke-HSR models, the RMSE values of the HM model are 41.7% and 66.7% lower, and the MRE values are 2.158% and 9.702% lower, respectively. Moreover, the HM model has the ability to improved the inadequate fitting outcomes of the Hapke-HSR model. These findings show that the HM model can describe SSR attributes more effectively than the other models can, especially at SMC ≥ 30%. The key factor is that the HM model combines the strengths of both the Hapke-HSR and MARMIT-2 models to better describe the changes in SSR with increasing SMC. The MARMIT-2 model also exhibits higher accuracy at SMC ≥ 30% since it fully considers the effect of the SMC on SSR.

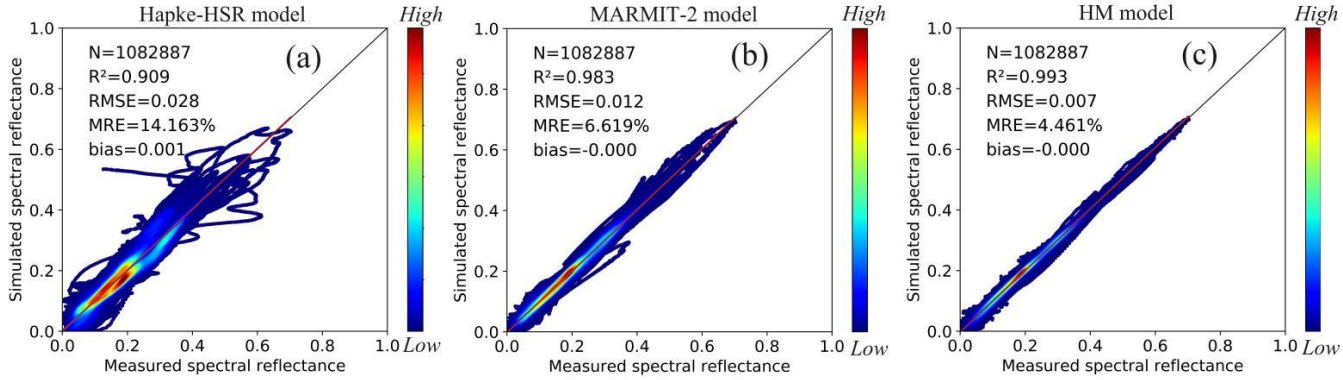

Figure 7: Comparison results of the soil reflectance values simulated by the Hapke-HSR (a), MARMIT-2 (b) and Hapke-HSR + MARMIT-2 (HM) (c) models with the measured soil reflectance at SMC ≥ 30%.

Next, we further evaluate the ability of the Hapke-HSR, MARMIT-2 and HM models to fit the measured SSR for different bands (0.4-2.5 μm) at SMC ≥ 30%. Figure 8 shows the comparison results between the simulated SSR values of the three models and the measured SSR values. The results of these three models are highly consistent with the measured values.

The R^2 values of these three models are generally very high, in the range of 0.4–2.5 μm. The R^2 value of the HM model is the largest, followed by those of the MARMIT-2 model and, finally, the Hapke-HSR model. However, the consistency between the outcomes of these three models and the measured values in the strong absorption band of water (centred at 1.90 μm) is significantly lower than that for the other bands. The RMSE results from the HM model were the smallest, followed by those of the MARMIT-2 model. The maximum RMSE value of the Hapke-HSR model was approximately 0.05 because the Hapke-HSR model uses a simplistic assumption to reflect the effect of the SMC. However, the HM and MARMIT-2 models significantly outperform the Hapke-HSR model, specifically at two major absorption bands of water (centred at 1.47 and 1.90 μm), since the HM and MARMIT-2 models fully consider the changes in SSR characteristics with variations in the SMC. The MRE trends of the three models are basically similar to the RMSE trends, and the HM model demonstrates the highest level of accuracy, with the MARMIT-2 model following closely behind. The MRE value of the Hapke-HSR model is approximately 60% at the major absorption band of water (centred at 1.90 μm), which is significantly greater than that of the MARMIT-2 model (28%) and the HM model (15%). The bias values of the HM model approach 0.4–2.5 μm, whereas those of the Hapke-HSR model exhibit a large range of variation. These studies indicate that the HM model results are more in line with the fitted SSR, whereas the Hapke-HSR model results are more different from the measured SSR values. In general, the variations between the outputs of these three models and the measured values are in the wavelength ranges of 0.4–0.6 μm and 2.4–2.5 μm and represent the two major absorption bands of water. The soil reflectance is low over the spectral region from 0.40.6 μm, and the soil reflectance variation remains insignificant in this wavelength range as the SMC increases. The soil measurements have great uncertainty in the range of 2.4–2.5 μm, resulting in poor correlations between the fitting results of these three models and the measured values. The SSR changes rapidly in the strong absorption band of water, which leads to great uncertainty in the fitting results of these models. Compared with the observed SSR model, the Hapke-HSR model has the lowest accuracy, followed by the MARMIT-2 model. The HM and MARMIT-2 models are better than the Hapke-HSR model at SMC ≥ 30% because these two models fully consider the variation in SSR characteristics with the variation in SMC.

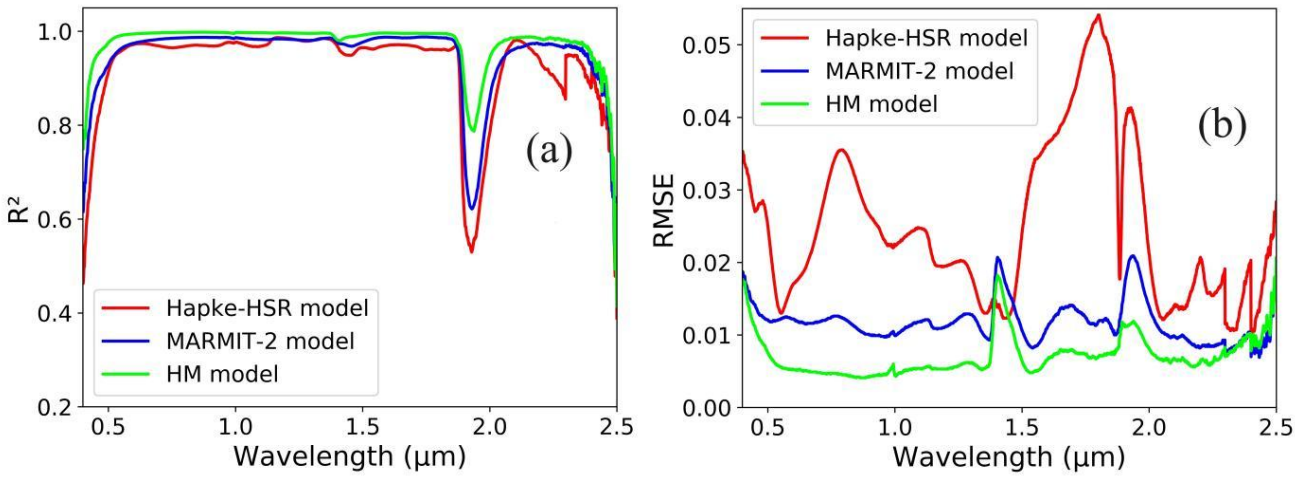

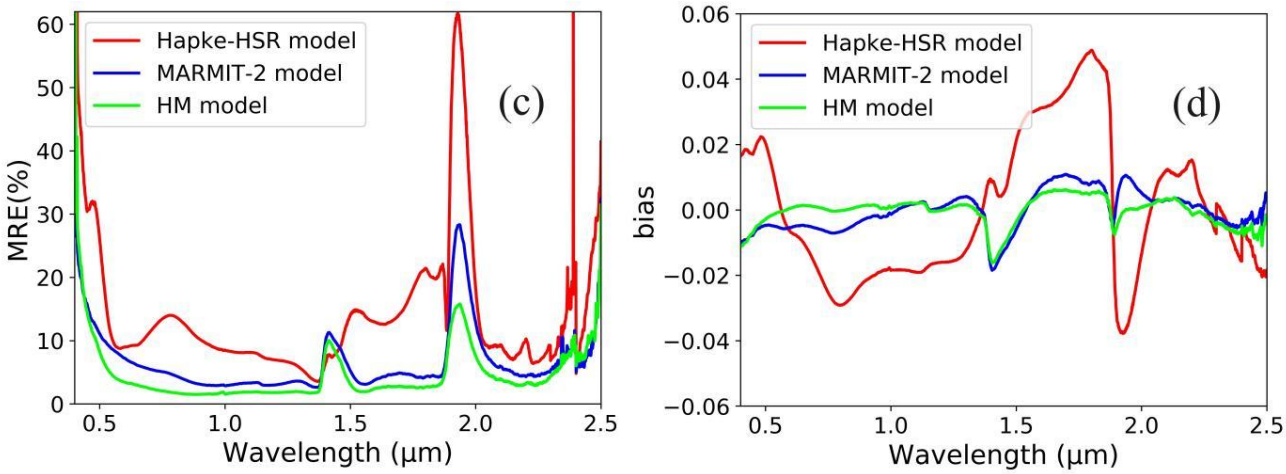

Figure 8. Evaluation of the Hapke-HSR (red), MARMIT-2 (blue) and Hapke-HSR + MARMIT-2 (HM) (lime) models in fitting measured soil reflectance at SMC ≥ 30%. The assessment indices are the R^2 (a), RMSE (b), MRE (c), and bias (d) values.

Finally, we analysed the fitting performance of the Hapke-HSR, MARMIT-2, and HM models across eight soil spectral databases, as shown in Figure 9. All three models achieve high accuracy (NRMSE < 9%), with the HM model generally outperforming the individual models. The performance varies across datasets, reflecting differences in soil properties, reflectance levels, and sensitivity to soil moisture. The HM model shows clear improvements for most datasets (e.g., Bab16, Dup20, Hum15, Liu02, Mar12, and Phil14), indicating the effectiveness of coupling directional scattering and moisture-related processes. However, the improvement is less pronounced for certain datasets. For example, the MARMIT-2 model already achieves high accuracy for the Les08 dataset, resulting in limited additional improvement. For the Lob02 dataset, the relatively low reflectance leads to larger NRMSE values, which reduces the apparent gain. Overall, these results demonstrate the robustness of the proposed framework across diverse datasets, while also highlighting its dependence on dataset characteristics.

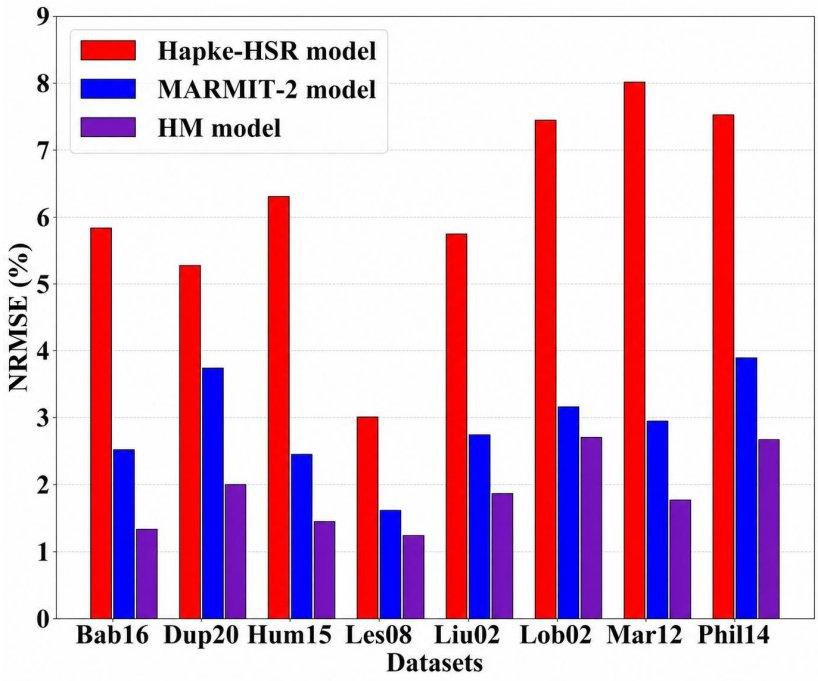

Figure 9: The NRMSE values of the measured soil reflectance fit with the Hapke-HSR (red), MARMIT-2 (blue) and Hapke-HSR + MARMIT-2 (HM) (lime) models for eight different databases.

5 Discussion

5.1 Analysis of the variation in the parameter χ_{soil}

In this section, we analyse the imaginary component of the soil index (χ_{soil} parameter) calculated from the dry soil reflectance for eight different databases with the wavelengths shown in Figure 10. For different soil databases, the change trend of the χ_{soil} parameter is basically the same. The χ_{soil} parameter increases with wavelength, and there is an obvious peak at the two strong absorption bands of water (i.e., centred at 1.47 and 1.90 μm). However, there are still some differences between different soil databases. The values of the parameter χ_{soil} are greater in the strong absorption band of water for the Bab16 and Liu02 databases, whereas the parameter values χ_{soil} are lower for the Hum15, Lob02 and Phil14 databases in the strong absorption band of water; moreover, the influence of the SMC on these three databases is small. For the same soil database, the change in the parameter χ_{soil} is small, and only the difference between the Bab16 database results is large. In addition, the parameter χ_{soil} is obviously greater in the two water absorption bands, and the overall change range also decreases. This decrease may further affect the accuracy of fitting the measured SSR. Therefore, the method of determining the parameter χ_{soil} in each soil database should be theoretically feasible. The parameter χ_{soil} is derived based on the assumption that the spectral shape of dry soil reflectance is similar to that of the single scattering albedo. Therefore, this approach depends on the availability of dry soil reflectance, which is often difficult to obtain from field measurements or satellite observations. Providing a representative dry soil reflectance remains an important challenge for future work. In addition, the use of an averaged χ_{soil} does not explicitly account for variability in soil properties within the same soil type, such as differences in organic carbon content or texture, which may influence spectral absorption. This simplification may contribute to the observed decrease in model accuracy. In future work, the definition of χ_{soil} could be refined by incorporating soil-specific properties or by grouping spectrally similar soils, which is expected to provide a more accurate representation of absorption characteristics and further improve model performance.

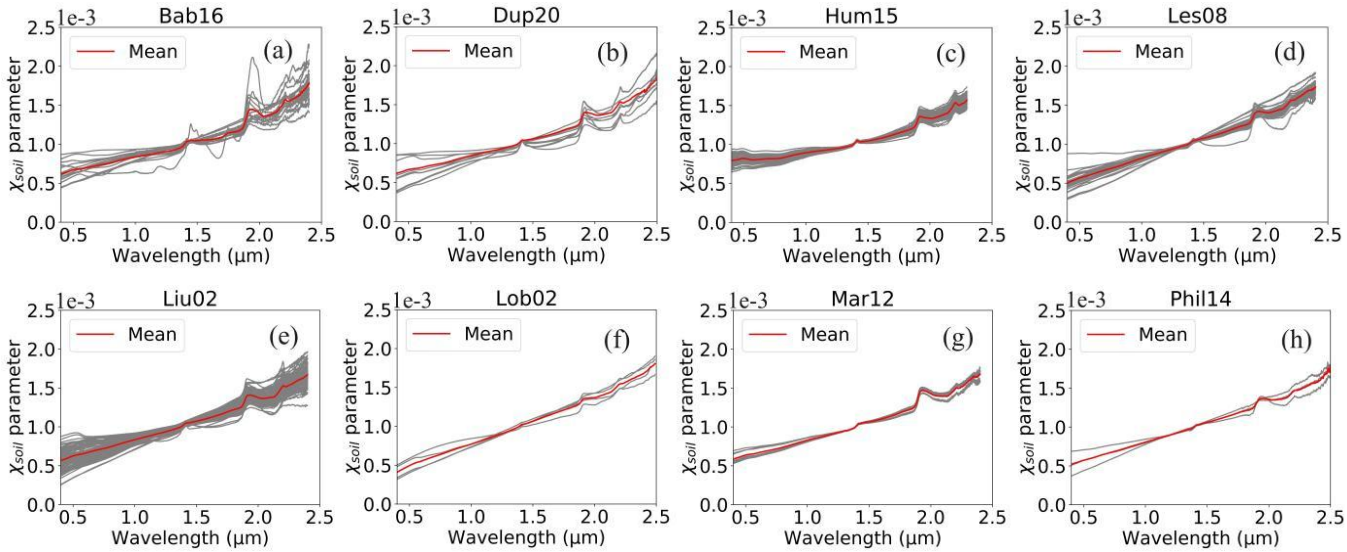

Figure 10: Analysis of the imaginary component of the soil index (parameter χ_{soil}) for eight different databases (i.e., Bab16 (a), Dup20 (b), Hum15 (c), Les08 (d), Liu02 (e), Lob02 (f), Mar12 (g), and Phil14 (h)) with wavelengths.

5.2 Validating the Hapke-HSR + MARMIT-2 model using the average parameter χsoil

We used the average parameter χ_{soil} (i.e., Figure 10(a)) to validate the HM model to characterize the SSR attributes; this model is called the HM_mean model in the following section. Figure 11 shows that the HM and HM_mean models fit the influence of the typical measured SSR value (i.e., bab16_056-051) at SMC = 0%, 9.1%, 17%, 29.9%, 39.3%, and 52.4%,

respectively. This set of typical data is thought to have a specular reflection effect when SMC = 52.4%. The HM and HM_mean models match well with the typical measured SSR values. However, the HM model shows greater consistency with the fitted SSR value than does the HM_mean model, especially at SMC < 10%. The HM_mean model results in significant underestimation and overestimation at SMC = 0% and 9.1%, respectively, because the average parameter χ_{soil} is obviously greater in the water absorption band (Figure 10(a)), which further affects the accuracy of the HM_mean model. The HM and HM_mean model fitting results can capture the change in SSR with increasing SMC and are highly in line with the measured SSR values at high SMCs, which may be caused by the obvious SSR broadening in the strong absorption band of water with increasing SMC. In general, the HM model, which uses the average parameter χ_{soil}, can still effectively describe the SSR characteristics, especially at high SMCs. However, the average parameter χ_{soil} leads to a significant broadening of the strong absorption band of water at low SMCs, which further leads to obvious overestimation or underestimation of the SSR fitted by the HM_mean model in the strong absorption band of water.

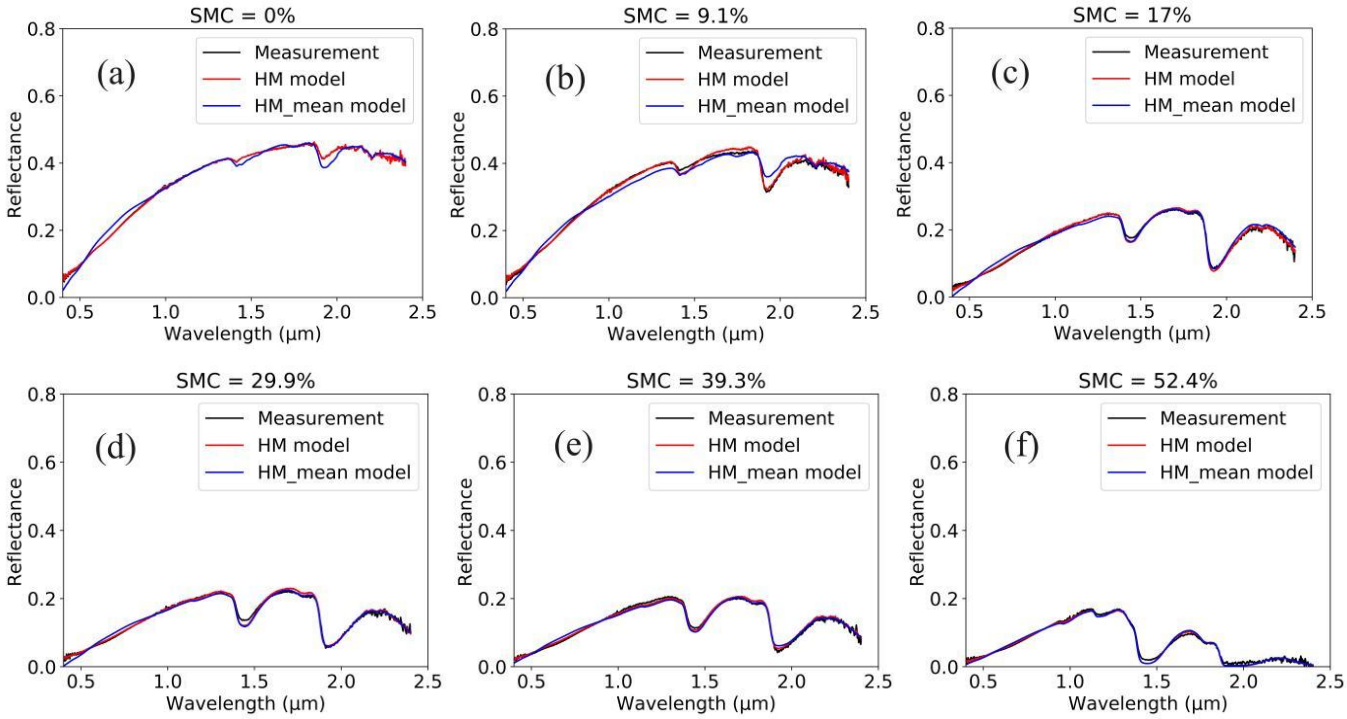

Figure 11: The HM (red) and HM_mean (blue) models fit the measured soil reflectance (black) at SMC = 0% (a), 9.1% (b), 17% (c), 29.9% (d), 39.3% (e), and 52.4% (f).

Table 6. The HM and HM_mean models fit the soil reflectance variables and statistical outputs.

Models	SMC	*b*	*M*	*δ*	*L*	*ε*	R^2	RMSE	bias
HM model	0.0	2.0	0.30	0.00	0.00	0.0	1.000	0.001	0.000
	9.1	3.6	0.22	0.14	0.01	0.2	0.996	0.007	0.003
	17.0	1.8	0.32	0.05	0.01	0.6	0.993	0.006	0.000
	29.9	2.2	0.28	0.07	0.02	0.6	0.990	0.006	0.001
	39.3	1.2	0.38	0.06	0.02	0.6	0.990	0.006	0.001
	52.4	1.8	0.32	0.01	0.05	0.9	0.991	0.005	-0.002
	All	--	--	--	--	--	0.998	0.005	0.001
HM_mean model	0.0	2.2	0.18	0.04	0.00	0.9	0.989	0.012	0.001
	9.1	2.2	0.18	0.14	0.00	1.0	0.977	0.016	-0.001
	17.0	0.6	0.34	0.13	0.01	0.6	0.980	0.009	0.002

	29.9	0.6	0.34	0.09	0.02	0.6	0.981	0.008	-0.001
	39.3	1.0	0.26	0.10	0.03	0.6	0.981	0.008	0.000
	52.4	2.6	0.16	0.03	0.06	0.9	0.988	0.006	-0.002
	All	--	--	--	--	--	0.993	0.011	0.000

Table 6 shows that the HM and HM_mean models fit the SSR parameters and statistical outputs. The overall accuracy of the HM and HM_mean models in terms of fitting the measured SSR is high (R^2 = 0.991–0.993, RMSE = 0.005–0.011). According to the simulation results, the HM model is more accurate with respect to the measured SSR than the HM_mean model is, especially at SMC < 10%, because the average parameter χ_{soil} is obviously greater in the water absorption band. The HM and HM_mean models can effectively describe SSR features, especially high SMCs (R^2 > 0.98 and RMSE < 0.01). When SMC = 52.4%, the measured soil spectral data are suspected to have a specular reflection effect, and the HM model maintains a higher fitting accuracy (R^2 = 0.991, RMSE = 0.005) than does the Hapke_mean model (R^2 = 0.988, RMSE = 0.006). These results indicate that the method of assuming an average parameter χ_{soil} in each soil database should be theoretically feasible. However, all the soil types may have large differences in the parameter χ_{soil}. How to select the parameter χ_{soil} of each soil type will be particularly important in our subsequent study.

Finally, we calculate the overall average parameter χ_{soil} to determine the dependence of the HM model on the dry SSR. First, we normalize all χ_{soil} parameters to the same order of magnitude and then average these indices in each band. Finally, we use all the SSR data to verify the accuracy of this method. Table 7 shows that the HM_mean model fit the statistical results for all the SSR data. Compared with the measured SSR, the HM_mean model has high fitting accuracy. The R^2 value of the HM_mean model is 0.988, and the RMSE is 0.014, indicating negligible bias. However, the fitting accuracy of the overall SSR data of the HM_mean model is lower than that of the MARMIT-2 and HM models (i.e., Figure 6(b)-(c)). The main reason is that there are notable discrepancies in the parameter χ_{soil} among various soil types (Figure 10). The model operation can be simplified by averaging all the χ_{soil} parameters of the soil, but this approach also results in an accuracy decline for the HM_mean model. For SMC values ≥ 30%, the HM_mean model results in a lower RMSE than that for SMC values < 30%, which is consistent with the findings illustrated in Figure 11 and Table 6. However, the NRMSE and MRE values of the HM_mean model at SMC ≥ 30% were lower than those at SMC < 30%, possibly because the dry SSR is greater than that of wet soil. In conclusion, the HM_mean model demonstrates proficiency in describing SSR attributes, and the overall average parameter χ_{soil} of the soil can be used to determine the dependence of the HM model on the SSR. In this study, we based our analysis solely on the soil databases, which has limitations. In future research, we will consider soil properties or spectrally similar soils and account for more factors affecting the χ_{soil} parameter to improve the accuracy of the Hapke-HSR + MARMIT-2 model.

Table 7. The HM_mean model fit the statistical results for all the soil reflectance data.

Data	Number	R^2	RMSE	NRMSE (%)	MRE (%)	bias
SMC < 30%	2257585	0.989	0.015	1.811	5.117	0.000
SMC ≥ 30%	1082887	0.980	0.013	1.858	6.988	0.000
All	3340472	0.988	0.014	1.743	5.723	0.000

5.3 Analysing the Parameter Influence of the Hapke-HSR + MARMIT-2 model on the soil BRDF shape

Finally, we analyse the impact of the soil parameters on the BRDF shape obtained with the Hapke-HSR + MARMIT-2 model. Considering that we previously used various BRDF data sources to examine the role of the Hapke-HSR model in modelling soil BRDF features, we analyse how the model parameters affect the shape of the BRDF curve (Ding et al., 2022). Figure 12 shows the effects of parameters b, M, δ, L and ε in the Hapke-HSR + MARMIT-2 (HM) model on the soil BRDF

shape in the principal plane (PP). With increasing parameter b, the soil reflectance gradually decreases in the forwards direction but increases in the backwards reflection direction. The parameter b has a relatively large contribution to the anisotropy characteristics of the soil. When the parameter M increases, the soil reflectance continuously decreases. The soil anisotropy is strongest when the parameter M is relatively small. With the increase in the parameter δ, the impact of the parameter δ on the soil reflectance is relatively large in the range of 0-0.01, and the anisotropy of the soil is strong; however, the influence of the parameter δ on the SSR is relatively low, and the soil anisotropy is significantly weak. As the parameter L increases, L does not impact the soil reflectance, which corresponds with the results in Figure 3(g). With increasing value of the parameter ε, the equal interval of the soil reflectance decreases since the influence of the surface coverage fraction of water is proportionally related to this factor. In summary, the variation in the parameters b and M in the Hapke-HSR model has a notable effect on the soil BRDF shape, whereas the parameters of the MARMIT-2 model have a relatively minimal effect on the soil BRDF shape. Therefore, the ability of the HM model to describe the features of the soil BRDF is basically consistent with that of the Hapke-HSR model. This occurs because the MARMIT-2 model does not include additional BRDF-related information, whereas the Hapke-HSR model includes input parameters for angle-related information. In future studies, we will comprehensively assess the ability of the HM model to represent soil BRDF features, especially in the forwards direction for wet soil.

Compared with existing models, the proposed Hapke-HSR + MARMIT-2 model provides a physically consistent integration of directional scattering and moisture-related processes. Semi-empirical models such as the BSM and general spectral vectors (GSV) capture spectral variability but lack explicit representation of angular effects (Ding et al., 2022; Jiang et al., 2019), which is critical for multi-angular observations and physically based parameter inversion. Moreover, soil reflectance acts as a key background component in canopy reflectance and influences vegetation parameter retrieval. By improving its spectral and directional representation under varying moisture conditions, the proposed framework can provide more reliable inputs for coupled soil–vegetation models (e.g., PROSAIL), thereby reducing uncertainties in vegetation parameter inversion. This study has certain limitations. To simplify the analysis, the effects of surface roughness and porosity are not explicitly considered (Ding et al., 2023, 2026). Despite this, the model achieves high accuracy, indicating its effectiveness in representing soil reflectance. The evaluation is conducted under a fixed observation geometry due to dataset limitations, which may constrain the characterization of angular effects. Nevertheless, the framework inherently accounts for viewing geometry through the Hapke formulation and can be extended to varying observation conditions. Future work will incorporate multi-angular datasets to further evaluate model performance.

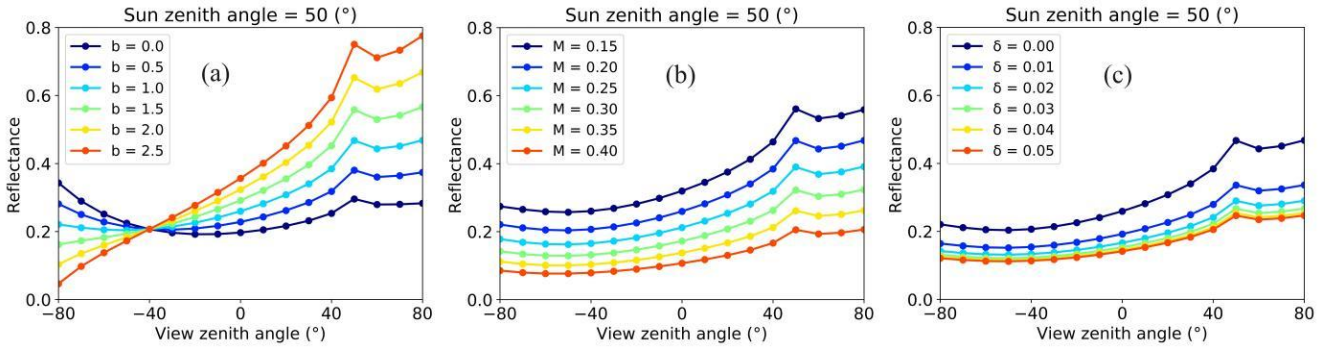

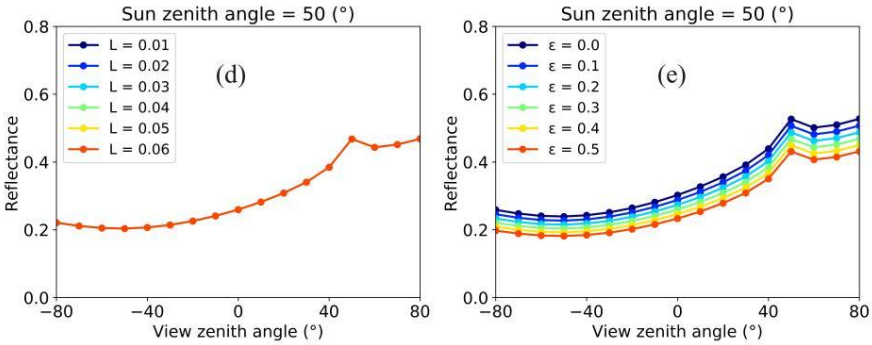

Figure 12: Influence of the coefficient of *b* (a), soil particle size and shape-dependent *M* (b), volume fraction *δ* (c), thickness *L* (d) and surface coverage fraction of water *ε* (e) parameters of the Hapke-HSR + MARMIT-2 (HM) model on the soil BRDF shape in the red band (0.67 µm).

6 Conclusion

This study develops a unified soil radiative transfer framework by refining the improved Hapke-HSR model and dynamically coupling it with the MARMIT-2 model to improve the representation of soil reflectance under varying soil moisture conditions. The primary objective is to overcome the limitations of the Hapke-HSR model in wet soils and the dependence of MARMIT-2 model on externally prescribed dry reflectance, thereby extending the applicability of both models.

First, dry SSR is used to estimate the imaginary part of the soil refractive index (χ_{soil}), which alleviates the piecewise fitting limitation of the Hapke-HSR model by establishing a continuous statistical relationship between single scattering albedo and wavelength. The improved Hapke-HSR is then coupled with MARMIT-2 to integrate particle scattering and moisture-dependent absorption processes within a physically consistent framework. The proposed Hapke-HSR + MARMIT-2 (HM) model is evaluated using multiple independent soil spectral databases. The results show that all three models reproduce measured SSR with reasonable accuracy, whereas the coupled HM model achieves consistently higher performance (R^2 = 0.993, RMSE = 0.007) than MARMIT-2 (R^2 = 0.983, RMSE = 0.012) and Hapke-HSR (R^2 = 0.909, RMSE = 0.028), with particularly pronounced improvements at high soil moisture levels (SMC ≥ 30%). This study does not aim to replace the MARMIT-2 model, which already provides an effective description of moisture effects, but rather to improve the overall physical consistency of soil reflectance modeling through the integration of complementary mechanisms. The coupled framework provides a robust basis for future developments in soil parameter inversion, particularly for soil moisture, and for improved representation of soil background effects in land-surface radiative transfer modeling.

In summary, this work addresses two key modeling challenges: (1) improving the hyperspectral consistency of the Hapke-HSR using dry soil reflectance, and (2) establishing a unified coupling strategy that jointly represents spectral behavior and moisture-dependent effects. The proposed framework contributes to the theoretical and methodological foundation of soil radiative transfer modeling and supports future advances in optical remote sensing of land-surface parameters.

Code and data availability. The Hapke-HSR + MARMIT-2 model code and example datasets used in this study are archived on Zenodo (https://doi.org/10.5281/zenodo.18366791; Ding, 2025). The original soil databases are derived from the MARMIT framework (https://pss-gitlab.math.univ-paris-diderot.fr/marmit/marmit).

Author contributions. Conceptualization, Anxin Ding, Shunlin Liang; methodology, Anxin Ding, Han Ma, Shunlin Liang, Ziti Jiao and Alexander A. Kokhanovsky; formal analysis, Anxin Ding, Han Ma and Rui Xie; data curation, Han Ma, Ziti Jiao and Rui Xie; software, Han Ma; investigation, Ziti Jiao; theoretical support, Alexander A.Kokhanovsky; data processing and validation, Hanyu Shi; supervision, Shunlin Liang; writing—original draft, Anxin Ding; writing—review and editing, Han Ma, Shunlin Liang, Ziti Jiao, Hanyu Shi, Alexander A.Kokhanovsky and Rui Xie.

Competing interests. The authors have no conflict of interest.

Acknowledgments. This study was supported by the National Natural Science Foundation of China (Grant No. 42301363) and the Anhui Province Youth Science and Technology Talent Lift Program (Grant No. RCTJ202404). We gratefully acknowledge Stéphane Jacquemoud and his team for sharing the implementation of the MARMIT-2 model, which provided valuable support for this study.

Appendix

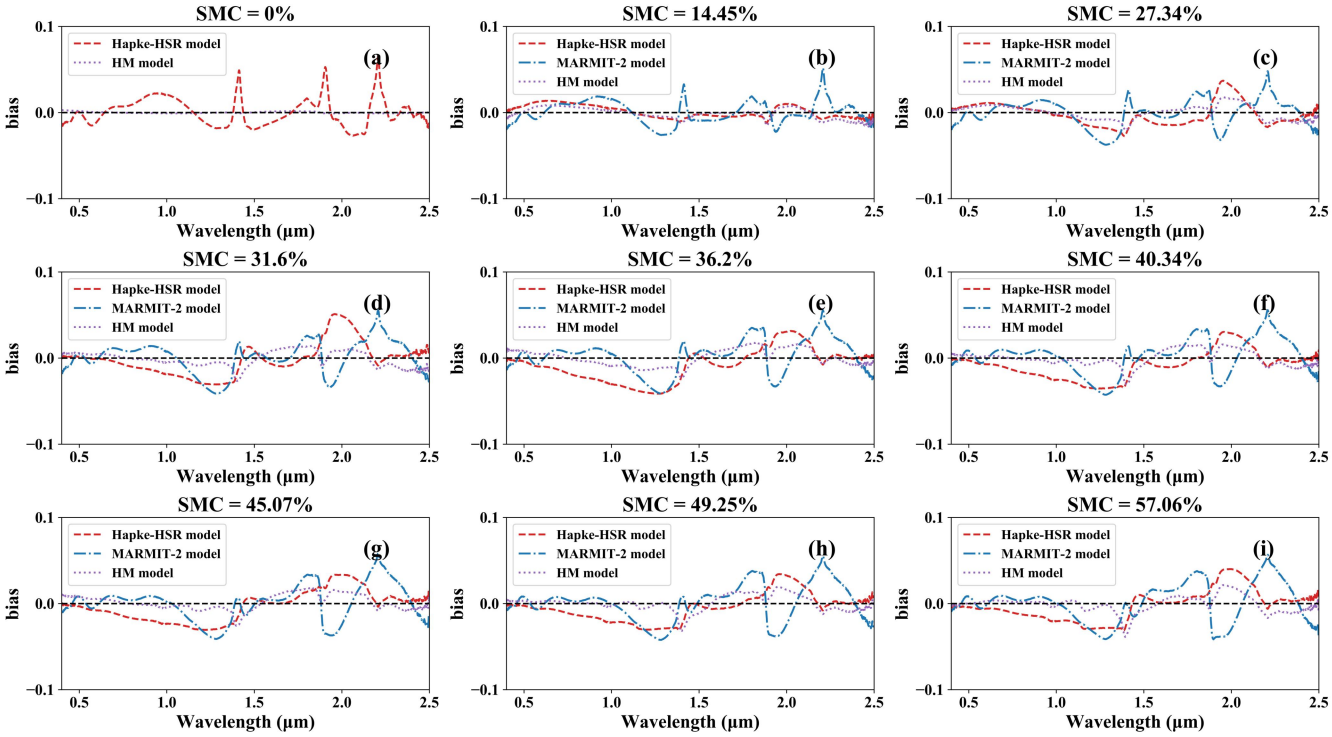

Figure A1: The bias (i.e., simulated reflectance of these models - measured reflectance) between the simulated spectral reflectance of the Hapke-HSR (red), MARMIT-2 (blue) and Hapke-HSR + MARMIT-2 (HM) (lime) models and the fitted soil reflectance at SMC = 0% (a), 14.45% (b), 27.34% (c), 31.6% (d), 36.2% (e), 40.34% (f), 45.07% (g), 49.25% (h), and 57.06% (i).

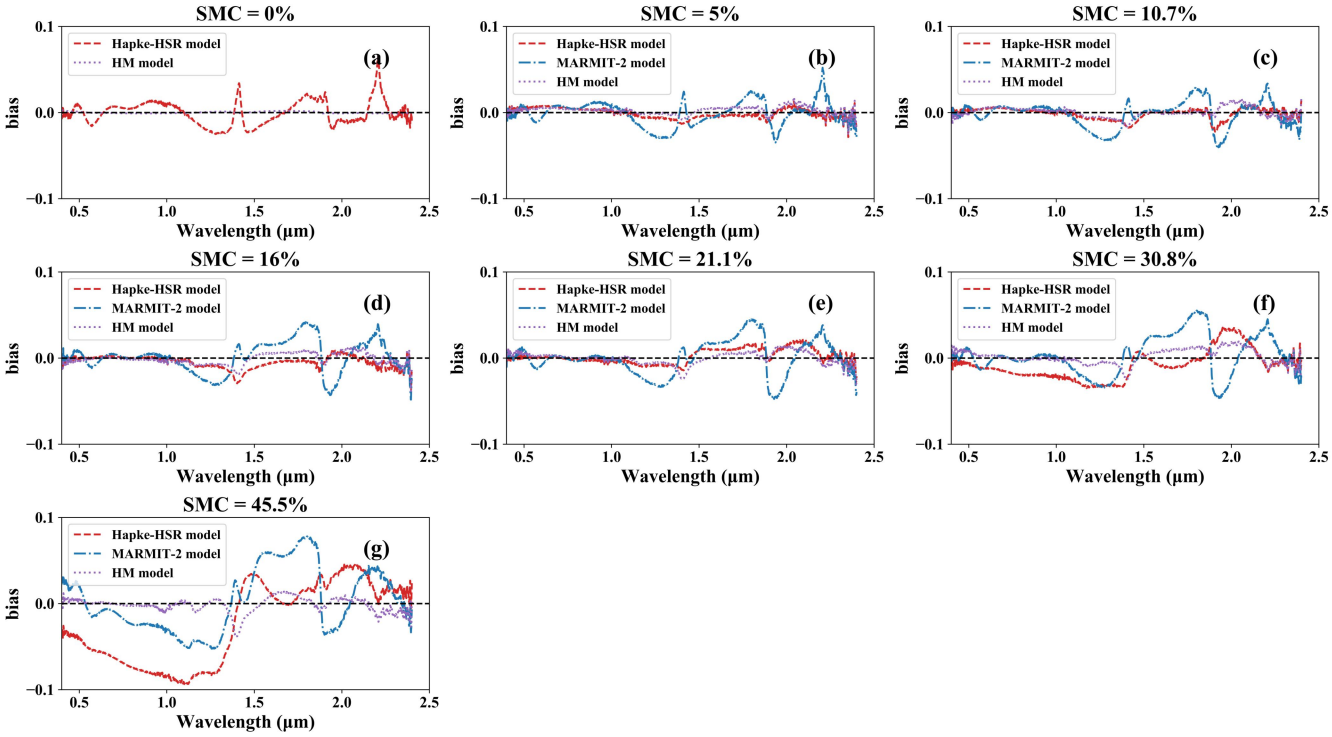

548

549 **Figure A2. The bias (i.e., simulated reflectance of these models - measured reflectance) between the simulated**
550 **reflectance of the Hapke-HSR (red), MARMIT-2 (blue) and Hapke-HSR + MARMIT-2 (HM) (lime) models and the**
551 **fitted soil reflectance at SMC = 0% (a), 5% (b), 10.7% (c), 16% (d), 21.1% (e), 30.8% (f), and 45.5% (g).**

552 **References**

553 Ångström, A.: The albedo of various surfaces of ground, Geografiska Annaler Series A: Physical Geography, 7, 323–342,
554 1925.
555 Bablet, A., Vu, P. V. H., Jacquemoud, S., Viallefont-Robinet, F., Fabre, S., Briottet, X., Sadeghi, M., Whiting, M. L., Baret,
556 F., and Tian, J.: MARMIT: a multilayer radiative transfer model of soil reflectance to estimate surface SMC in the solar
557 domain 400–2500 nm, Remote Sens. Environ., 217, 1–17, 2018. https://doi.org/10.1016/j.rse.2018.07.031.
558 Bach, H. and Mauser, W.: Modeling and model verification of the spectral reflectance of soils under varying moisture
559 conditions, IGARSS, 4, 2354–2356, 1994.
560 Cheng, J., Wen, J., Xiao, Q., Wu, S., Hao, D., and Liu, Q.: Extending the GOSAILT model to simulate sparse woodland
561 bidirectional reflectance with soil reflectance anisotropy consideration, Remote Sens., 14, 1001, 2022.
562 Ding, A., Ma, H., Liang, S., and He, T.: Extension of the Hapke model to the spectral domain to characterize soil physical
563 properties, Remote Sens. Environ., 269, 112843, 2022. https://doi.org/10.1016/j.rse.2021.112843.
564 Ding, A., Jiao, Z., Qi, J., Guo, J., Yang, P., Dong, Y., Zhang, X., Zhang, G., and Chen, J. M.: HBiM2: A multi-angle
565 hyperspectral soil radiative transfer model for simulating the reflectance of dry and wet soils. Remote Sens. Environ., 339,
566 115381, 2026. https://doi.org/10.1016/j.rse.2026.115381.
567 Ding, A., Jiao, Z., Zhang, X., Dong, Y., Kokhanovsky, A.A., Guo, J., & Jiang, H. 2023. A practical approach to improve the
568 MODIS MCD43A products in snow-covered areas. Journal of Remote Sensing, 3, 0057.
569 Dupiau, A., Jacquemoud, S., Briottet, X., Fabre, S., Viallefont-Robinet, F., Philpot, W., Di Biagio, C., Hébert, M., and
570 Formenti, P.: MARMIT-2: an improved version of the MARMIT model to predict soil reflectance as a function of surface
571 water content in the solar domain, Remote Sens. Environ., 272, 112951, 2022. https://doi.org/10.1016/j.rse.2022.112951
572 Fan, D., Zhao, T., Jiang, X., García-García, A., Schmidt, T., Samaniego, L., Attinger, S., Wu, H., Jiang, Y., Shi, J., Fan, L.,
573 Tang, B. H., Wagner, W., Dorigo, W., Gruber, A., Mattia, F., Balenzano, A., Brocca, L., Jagdhuber, T., Wigneron, J. P.,

Montzka, C., and Peng, J.: A Sentinel-1 SAR-based global 1 km resolution soil moisture data product: algorithm and preliminary assessment, Remote Sens. Environ., 318, 114579, 2025. https://doi.org/10.1016/j.rse.2024.114579.

Gao, S., Yan, K., Liu, J., Pu, J., Zou, D., Qi, J., and Yan, G.: Assessment of remote-sensed vegetation indices for estimating forest chlorophyll concentration, Ecol. Indic., 162, 112001, 2024. https://doi.org/10.1016/j.ecolind.2024.112001.

Gholami, B. N. and Mobasheri, M. R.: Influence of soil texture on the estimation of bare soil moisture content using MODIS images, Eur. J. Remote Sens., 51, 911–920, 2018.

Hapke, B.: Bidirectional reflectance spectroscopy 7: the single particle phase function hockey stick relation, Icarus, 221, 1079–1083, 2012. https://doi.org/10.1016/j.icarus.2012.10.022.

Jacquemoud, S.: Modeling spectral and bidirectional soil reflectance, Remote Sens. Environ., 41, 123–132, 1992. https://doi.org/10.1016/0034-4257(92)90072-R.

Jiang, C. and Fang, H.: GSV: a general model for hyperspectral soil reflectance simulation, Int. J. Appl. Earth Obs. Geoinf., 83, 101932, 2019. https://doi.org/10.1016/j.jag.2019.101932.

Jiang, H., Wei, X., Chen, Z., Zhu, M., Yao, Y., Zhang, X., and Jia, K.: Influence of different soil reflectance schemes on the retrieval of vegetation LAI and FVC from PROSAIL in agricultural regions, Comput. Electron. Agric., 12, 108165, 2023. https://doi.org/10.1016/j.compag.2023.108165.

Kimmel, B. W. and Baranoski, G. V. G.: A novel approach for simulating light interaction with particulate materials: application to the modeling of sand spectral properties, Opt. Express, 15, 9755–9777, 2007.

Labarre, S., Jacquemoud, S., Ferrari, C., Delorme, A., Derrien, A., Grandin, R., Jalludin, M., Lemaître, F., Métois, M., Pierrot-Deseilligny, M., Rupnik, E., and Tanguy, B.: Retrieving soil surface roughness with the Hapke photometric model: confrontation with the ground truth, Remote Sens. Environ., 225, 1–15, 2019.

Lekner, J. and Dorf, M. C.: Why some things are darker when wet, Appl. Opt., 27, 1278–1280, 1988.

Lei, T. and Bailey, B. N.: A text-based generative deep learning model for soil reflectance spectrum simulation in the solar range (400–2499 nm), Remote Sens. Environ., 318, 114527, 2025.

Li, L., Mu, X., Qi, J., Pisek, J., Roosjen, P., Yan, G., Huang, H., Liu, S., and Baret, F.: Characterizing reflectance anisotropy of background soil in open-canopy plantations using UAV-based multiangular images, ISPRS J. Photogramm. Remote Sens., 177, 263–278, 2021.

Liang, S. and Townshend, J. R. G.: A parametric soil BRDF model: a four-stream approximation for multiple scattering, Int. J. Remote Sens., 17, 1303–1315, 1996.

Liang, S. and Townshend, J. R. G.: A modified Hapke model for soil bidirectional reflectance, Remote Sens. Environ., 55, 1–10, 1996.

Ma, H., Liang, S., Xiao, Z., and Shi, H.: Simultaneous inversion of multiple land surface parameters from MODIS optical-thermal observations, ISPRS J. Photogramm. Remote Sens., 128, 240–254, 2017. https://doi.org/10.1016/j.isprsjprs.2017.04.007.

Ma, H., Liu, Q., Liang, S., and Xiao, Z.: Simultaneous estimation of leaf area index, fraction of absorbed photosynthetically active radiation, and surface albedo from multiple-satellite data, IEEE Trans. Geosci. Remote Sens., 55, 4334–4354, 2017.

Ni, W. and Li, X.: A coupled vegetation–soil bidirectional reflectance model for a semiarid landscape, Remote Sens. Environ., 74, 113–124, 2000.

Nolin, A. W. and Liang, S.: Progress in bidirectional reflectance modeling and applications for surface particulate media: snow and soils, Remote Sens. Rev., 18, 307–342, 2000.

Rizzo, R., Wadoux, A. M. J.-C., Demattê, J. A. M., Minasny, B., Barrón, V., Ben-Dor, E., Francos, N., Savin, I., Poppiel, R., Silvero, N. E. Q., Terra, F. S., Rosin, N. A., Rosas, J. T. F., Greschuk, L. T., Ballester, M. R. V., Gómez, A. M. R., Belllinaso, H., Safanelli, J. L., Chabrillat, S., Fiorio, P. R., Das, B. S., Malone, B. P., Zalidis, G., Tziolas, N., Tsakiridis, N., Karyotis, K., Samarinas, N., Kalopesa, E., Gholizadeh, A., Shepherd, K. D., Milewski, R., Vaudour, E., Wang, C., and

Salama, E. S. M.: Remote sensing of the Earth's soil color in space and time, Remote Sens. Environ., 299, 113845, 2023. https://doi.org/10.1016/j.rse.2023.113845.

Sadeghi, M., Babaeian, E., Tuller, M., and Jones, S. B.: The optical trapezoid model: a novel approach to remote sensing of soil moisture applied to Sentinel-2 and Landsat-8 observations, Remote Sens. Environ., 198, 52–68, 2017. https://doi.org/10.1016/j.rse.2017.05.041.

Sadeghi, M., Jones, S. B., and Philpot, W. D.: A linear physically based model for remote sensing of soil moisture using shortwave infrared bands, Remote Sens. Environ., 164, 66–76, 2015.

Sheng, Y., Sun, Z., Lu, S., and Omasa, K.: Ratio of physical model parameters can retrieve aggregate size from different types of soil in cultivated regions, Soil Tillage Res., 244, 106262, 2024. https://doi.org/10.1016/j.still.2024.106262.

Shoshany, M., Roitberg, E., Goldshleger, N., and Kizel, F.: Universal quadratic soil spectral reflectance line and its deviation patterns' relationships with chemical and textural properties: a global database analysis, Remote Sens. Environ., 155, 198–230, 2022. https://doi.org/10.1016/j.rse.2022.113182.

Verhoef, W., Van der Tol, C., and Middleton, E. M.: Hyperspectral radiative transfer modeling to explore the combined retrieval of biophysical parameters and canopy fluorescence from FLEX–Sentinel-3 tandem mission multi-sensor data, Remote Sens. Environ., 204, 942–963, 2018. https://doi.org/10.1016/j.rse.2017.08.006.

Verhoef, W. and Bach, H.: Coupled soil–leaf–canopy and atmosphere radiative transfer modeling to simulate hyperspectral multi-angular surface reflectance and TOA radiance data, Remote Sens. Environ., 109, 166–182, 2007. https://doi.org/10.1016/j.rse.2006.12.013.

Xu, H., Sun, H., Xu, Z., Wang, Y., Zhang, T., Wu, D., and Gao, J.: kNDMI: a kernel normalized difference moisture index for remote sensing of soil and vegetation moisture, Remote Sens. Environ., 319, 114621, 2025. https://doi.org/10.1016/j.rse.2025.114621.

Yang, G. J., Zhao, C. J., Huang, W. J., and Wang, J. H.: Extension of the Hapke bidirectional reflectance model to retrieve soil water content, Hydrol. Earth Syst. Sci., 15, 2317–2326, 2011.

Yang, P.: Exploring the interrelated effects of soil background, canopy structure, and sun–observer geometry on canopy photochemical reflectance index, Remote Sens. Environ., 279, 113133, 2022. https://doi.org/10.1016/j.rse.2022.113133.

Yang, P., van der Tol, C., Liu, J., and Liu, Z.: Separation of the direct reflection of soil from canopy spectral reflectance, Remote Sens. Environ., 316, 114500, 2025. https://doi.org/10.1016/j.rse.2024.114500.

Zeng, Y., Hao, D., Badgley, G., Damm, A., Rascher, U., Ryu, Y., Johnson, J., Krieger, V., Wu, S., Qiu, H., Liu, Y., Berry, J. A., and Chen, M.: Estimating near-infrared reflectance of vegetation from hyperspectral data, Remote Sens. Environ., 267, 112723, 2021. https://doi.org/10.1016/j.rse.2021.112723.

Zhao, X., Qi, J., Xu, H., Yu, Z., Yuan, L., Chen, Y., and Huang, H.: Evaluating the potential of airborne hyperspectral LiDAR for assessing forest insects and diseases with 3D radiative transfer modeling, Remote Sens. Environ., 297, 113759, 2023. https://doi.org/10.1016/j.rse.2023.113759.